

TOPICAL REVIEW

The Muon Magnetic Moment and Supersymmetry

Dominik Stöckinger

School of Physics,
University of Edinburgh,
Edinburgh EH9 3JZ, UK

E-mail: dominik.stockinger@ed.ac.uk

Abstract.

The present review is devoted to the muon magnetic moment and its role in supersymmetry phenomenology. Analytical results for the leading supersymmetric one- and two-loop contributions are provided, numerical examples are given and the dominant $\tan\beta \operatorname{sign}(\mu)/M_{\text{SUSY}}^2$ behaviour is qualitatively explained. The consequences of the Brookhaven measurement are discussed. The 2σ deviation from the Standard Model prediction implies preferred ranges for supersymmetry parameters, in particular upper and lower mass bounds. Correlations with other observables from collider physics and cosmology are reviewed. We give, wherever possible, an intuitive understanding of each result before providing a detailed discussion.

PACS numbers: 12.60.Jv,13.40.Em,14.60.Ef

Contents

1	Introduction	1
1.1	Comparison of experiment and Standard Model theory	2
1.2	Relevant properties of the MSSM	4
1.3	Magnetic moment of the muon and chirality flips	9
2	Analytic results	10
2.1	How large can the SUSY contributions be?	10
2.2	One-loop contributions	13
2.3	Two-loop contributions	15
2.3.1	Two-loop corrections to SM one-loop diagrams	16
2.3.2	Two-loop corrections to SUSY one-loop diagrams	19
2.4	Summary of known contributions and error estimate	21
3	Numerical behaviour of the SUSY contributions	23
3.1	One-loop contributions	23
3.1.1	Dependence on mass parameters	24
3.1.2	CP violation and flavour violation	26
3.2	Two-loop contributions	27
3.2.1	Chargino/neutralino-loop contributions	27
3.2.2	Sfermion-loop contributions	29
3.3	Results for SPS benchmark points	31
4	Impact on SUSY phenomenology	32
4.1	Constraints from a_μ on the general MSSM	33
4.2	General correlations with other observables	35
4.2.1	B -decays	36
4.2.2	Neutralino dark matter density and detection rate	36
4.2.3	Lightest Higgs boson mass	37
4.2.4	Electroweak precision observables	38
4.3	MSUGRA	38
4.4	Gauge-mediated SUSY breaking	41
4.5	Anomaly-mediated SUSY breaking	42
4.6	MSSM parameter scan	43
5	Concluding remarks and outlook	45

1. Introduction

The magnetic moment of the muon is one of the most precisely measured and calculated quantities in elementary particle physics. It has been measured recently at Brookhaven National Laboratory to a precision of 0.54 parts per million (ppm) [1–6]. The Standard

Model (SM) theory prediction has reached a comparable level. Thanks to this fantastic precision the comparison of theory and experiment is not only a sensitive test of all SM interactions but also of possible new physics at the electroweak scale, which is typically suppressed by a factor $(m_\mu/M_{\text{new ph.}})^2$ and can be expected to contribute at the ppm-level.

Indeed, the experimental result [3] published in 2001 showed a 4 ppm deviation with a statistical significance of almost 3σ from the SM prediction. This caused a lot of enthusiasm and could be nicely explained by a variety of new physics scenarios at the weak scale, in particular by weak-scale supersymmetry (SUSY). In the meantime several errors in the SM prediction have been corrected, but due to smaller error bars on the theoretical and the experimental side, the current 2 ppm deviation still has a significance of more than 2σ (if the SM prediction is based on e^+e^- data, see below). Of course, this deviation does not rule out the SM. However, it is intriguing that SUSY, which is widely regarded as one of the most compelling ideas for physics beyond the SM, would naturally lead to a deviation of the observed magnitude.

In the present review we describe the rich interplay between SUSY and the magnetic moment of the muon. In section 2 we present the analytical results for the SUSY contributions at the one- and two-loop level and discuss their main features. In section 3 the numerical values of the SUSY contributions as functions of the SUSY parameters are analyzed. In section 4 we discuss the implications of the experimental result for the possible values of SUSY parameters and the correlations with other observables. In the remainder of this introduction we review the status of the comparison of experiment and SM theory and provide some necessary background on SUSY and on the theory of magnetic moments.

1.1. Comparison of experiment and Standard Model theory

The magnetic moment $\vec{\mu}$ of a particle with mass m and charge e is related to the particle spin \vec{S} by the gyromagnetic ratio g :

$$\vec{\mu} = g \left(\frac{e}{2m} \right) \vec{S}. \quad (1)$$

At tree level, QED predicts the exact result $g = 2$ for elementary spin- $\frac{1}{2}$ -particles such as electron and muon. Quantum effects from QED loop diagrams, from strong or weak interactions, or from hypothetical new particles lead to a deviation

$$a = \frac{1}{2}(g - 2), \quad (2)$$

the so-called anomalous magnetic moment. The theoretical prediction of the anomalous magnetic moment of a lepton with mass m is dominated by the one-loop QED contribution, the famous Schwinger term $\alpha/2\pi$ [7], followed by higher-order QED and strong interaction effects. Loop contributions from heavy particles with mass M are generally suppressed by a factor m^2/M^2 as explained below in section 1.3. Therefore, the anomalous magnetic moment of the muon is a factor $(m_\mu/m_e)^2 \approx 40\,000$ more sensitive to such contributions than the one of the electron.

The anomalous magnetic moment of the muon a_μ has been determined to an unprecedented precision of 0.54 parts per million (ppm) at the Brookhaven $g - 2$ experiment E821 [1–6]:

$$a_\mu^{\text{exp}} = 11\,659\,208.0(6.3) \times 10^{-10}. \quad (3)$$

This is the first magnetic moment measurement that is sensitive to effects from physics at the electroweak scale, and it has the potential to constrain and discriminate between models of physics beyond the Standard Model (SM).

Inspired by the success of this experiment, the SM theory prediction of a_μ has been considerably refined and scrutinized in the last few years (see e.g. [8–12] for recent reviews and references). The SM prediction can be decomposed into QED, hadronic and weak contributions. The QED contribution is the largest, but it is theoretically well under control. The weak contributions are the smallest SM contributions and amount to $15.4(0.2) \times 10^{-10}$, but they are relevant at the current level of experimental sensitivity. Their structure and numerical value are comparable to the ones of potential new physics contributions.

Currently, the hadronic contributions are the main source of the SM theory uncertainty. They can be decomposed according to the hadronic subdiagrams into vacuum polarization and light-by-light scattering contributions. The hadronic vacuum polarization contributions can be inferred from experimental data on the hadronic e^+e^- annihilation cross section using a dispersion relation. Thus ultimately the precision of these contributions is related to the precision of experimental data, which is constantly increasing due to ongoing measurements at Novosibirsk, B factories and the ϕ factory DAΦNE. The alternative method of determining the hadronic vacuum polarization from data on hadronic τ decays suffers from theory uncertainties that are difficult to assess and is not in perfect agreement with the e^+e^- -based results. The current relative accuracy of these contributions is about 1%, corresponding to 7.2×10^{-10} error in a_μ . The hadronic light-by-light contributions cannot be related to experimental data and are notoriously difficult to evaluate. Early evaluations had a sign error, identified in [13, 14], which led to a seemingly large deviation between the experimental result published in 2001 and the then current SM prediction [3]. Current estimates vary between $8.6(3.5) \times 10^{-10}$ [15] and $13.6(2.5) \times 10^{-10}$ [16].

For the purpose of the present review we will use the SM theory prediction given in [11], based on the most recent e^+e^- -based evaluations of the hadronic contributions [15, 17] (see [18] for another recent evaluation, leading to a similar result):

$$\begin{aligned} a_\mu^{\text{SM}} &= 11\,659\,184.1(7.2)^{\text{Vac.Pol.}}(3.5)^{\text{LBL}}(0.3)^{\text{QED/weak}} \times 10^{-10} \\ &= 11\,659\,184.1(8.0) \times 10^{-10}. \end{aligned} \quad (4)$$

Thus there is a deviation of about 2 ppm between the experimental result and the SM theory prediction:

$$\Delta a_\mu(\text{exp} - \text{SM}) = 23.9(9.9) \times 10^{-10}. \quad (5)$$

In order to appreciate the result further, we put it into historical context and compare it to the situation after the first measurement of a_μ at CERN in the 1970's,

with the result [19]

$$a_\mu^{\text{exp,1978}} = 11\,659\,240(85) \times 10^{-10}. \quad (6)$$

This experiment was the first to be sensitive to hadronic contributions to a_μ , so it was interesting to compare its result to the theory prediction without hadronic contributions and to the hadronic contributions individually,

$$\Delta a_\mu([\text{exp,1978}] - [\text{SM without had}]) = 720(85) \times 10^{-10}, \quad (7)$$

$$a_\mu^{\text{had,1978}} = 667(81) \times 10^{-10}, \quad (8)$$

where the central values and errors from Ref. [19] have been used. Without including the hadronic contributions there was a gap of more than 8σ between theory and experiment, but this gap was beautifully closed by the hadronic contributions. Hence the CERN experiment confirmed the existence of hadronic contributions to a_μ and the correctness of the SM with a high significance.

Likewise, the new Brookhaven experiment is the first to be sensitive to weak interaction effects, and it is instructive to compare its result to the SM prediction without weak contributions and the weak contributions individually,

$$\Delta a_\mu([\text{exp}] - [\text{SM without weak}]) = 39.3(9.9) \times 10^{-10}, \quad (9)$$

$$a_\mu^{\text{weak}} = 15.4(0.2) \times 10^{-10} \quad (10)$$

Again, without including the weak contributions there is a gap of about 4σ , which establishes the existence of contributions beyond the QED and hadronic effects. However, in this case the gap (9) is about 2.5 times larger than the SM weak contribution (10).

The deviation (5) or the difference between (9) and (10) has a significance of about 2.4σ . This is clearly not sufficient to prove the existence of physics beyond the SM. The deviation could be due to e.g. statistical fluctuations in the experimental result of a_μ itself or the experimental data leading to the prediction of $a_\mu^{\text{Vac.Pol.}}$, or the imperfect understanding of a_μ^{LBL} , or a combination of these effects.

Nevertheless, the result is tantalizing in view of new physics at the weak scale [20]. The existence of new physics at the weak scale has been suspected long before the a_μ measurement of (3), for reasons related e.g. to the naturalness problem of the SM Higgs sector, grand unification, or cosmology and dark matter. Generically, new physics at a scale M can be expected to contribute at the order m_μ^2/M^2 to a_μ , up to some numerical prefactors. For $M \sim M_W$ such a contribution could easily amount to 2 ppm, and this is just the magnitude of the observed deviation (5). In the following we focus on supersymmetry as a particularly well-motivated and predictive idea for physics beyond the SM.

1.2. Relevant properties of the MSSM

The deviation between experimental and theoretical value of a_μ could be due to contributions from supersymmetry. SUSY at the electroweak scale is one of the most

Table 1. The field/particle content of the MSSM. Only 2nd generation (s)leptons and 3rd generation (s)quarks are listed explicitly. The mass eigenstates corresponding to the electroweak gauge and Higgs bosons and their superpartners are indicated.

	(s)leptons	(s)quarks	Higgs Higgsinos	gauge bosons gauginos
SM/THDM	$\begin{pmatrix} \nu_\mu \\ \mu_L \end{pmatrix}, \mu_R, \dots$	$\begin{pmatrix} t_L \\ b_L \end{pmatrix}, t_R, b_R, \dots$	$\mathcal{H}_1, \mathcal{H}_2$	$B^\mu, W^{a\mu}; G^{a\mu}$ $\underbrace{\gamma, Z, W^\pm, G^{0,\pm}, h^0, H^0, A^0, H^\pm}$
SUSY partners	$\begin{pmatrix} \tilde{\nu}_\mu \\ \tilde{\mu}_L \end{pmatrix}, \tilde{\mu}_R, \dots$	$\begin{pmatrix} \tilde{t}_L \\ \tilde{b}_L \end{pmatrix}, \tilde{t}_R, \tilde{b}_R, \dots$	\tilde{H}_1, \tilde{H}_2	$\tilde{B}, \tilde{W}^a; \tilde{g}^a$ $\underbrace{\chi_{1,2,3,4}^0, \chi_{1,2}^\pm}$

compelling ideas of physics beyond the SM (see e.g. [21–25] for reviews). SUSY is the unique symmetry that relates fermions and bosons in relativistic quantum field theories. It eliminates the quadratic divergences associated with the Higgs boson mass and thus stabilizes the weak scale against quantum corrections from ultra-high scales. SUSY at the weak scale also automatically leads to gauge coupling unification, and the lightest SUSY particle (LSP) can be neutral and stable and constitutes a natural candidate for cold dark matter. Moreover, in contrast to many other scenarios for physics beyond the SM, the minimal supersymmetric standard model (MSSM) is a weakly coupled, renormalizable gauge theory [26], such that quantum effects are computable and well-defined, and it has survived many non-trivial electroweak precision tests [27].

The MSSM is the appropriate framework for a general discussion of a_μ and SUSY. The unknown supersymmetry breaking mechanism is parametrized in terms of a set of in principle arbitrary soft SUSY breaking parameters. Specific models of supersymmetry breaking can be accommodated within the MSSM by suitable restrictions on these parameters.

The MSSM as the minimal supersymmetric extension of the SM contains all SM particles and corresponding SUSY partners, see table 1. In addition it also contains a second Higgs doublet with associated SUSY partner; hence the MSSM can actually be regarded as the SUSY version of the two-Higgs-doublet model (THDM). Two Higgs doublets $\mathcal{H}_{1,2}$ of opposite hypercharge ∓ 1 are required for the cancellation of chiral gauge anomalies caused by the corresponding Higgsinos. Thus the field content of the MSSM comprises the THDM fields, including five physical Higgs bosons, see (31)–(33) below, scalar SUSY partners of each chiral SM fermion, called sfermions $\tilde{f}_{L,R}$, Higgsino doublets $\tilde{H}_{1,2}$, and U(1), SU(2) and SU(3) gauginos (called bino, winos and gluinos) $\tilde{B}, \tilde{W}^{\pm,3}, \tilde{g}$. Right-handed (s)neutrinos as well as non-vanishing neutrino masses are not relevant for this review and are ignored.

Two central MSSM parameters that are of particular importance for a_μ are related

to the two Higgs doublets. The first of these is the ratio of the two vacuum expectation values,

$$\tan \beta = \frac{v_2}{v_1}. \quad (11)$$

SUSY and gauge invariance require that the doublet \mathcal{H}_1 gives masses to down-type fermions, while \mathcal{H}_2 gives masses to up-type fermions. As a result, e.g. the top- and bottom-Yukawa couplings in the MSSM are enhanced by factors $1/\sin \beta$ and $1/\cos \beta$, respectively. In order to avoid non-perturbative values of these Yukawa couplings, $\tan \beta$ is commonly restricted to the range between about 1 and 50. High values $\tan \beta = \mathcal{O}(50)$ lead to similar top and bottom Yukawa couplings and are therefore favoured by the idea of top-bottom Yukawa coupling unification [28].

The second important parameter relating the two Higgs doublets is the μ -parameter, which appears in the MSSM Lagrangian in the terms

$$\mu \tilde{H}_1 \tilde{H}_2 - \mu F_{H_1} \mathcal{H}_2 - \mu F_{H_2} \mathcal{H}_1 + h.c.. \quad (12)$$

The first term describes a Higgsino mass term, while in the other terms $F_{H_{1,2}}$ are auxiliary fields whose elimination gives rise to interactions of $\mathcal{H}_{1,2}$ with sfermions of the opposite type compared to the Yukawa couplings, e.g. to $\mathcal{H}_1^0 \tilde{t}_L \tilde{t}_R^\dagger$ and $\mathcal{H}_2^0 \tilde{\mu}_L \tilde{\mu}_R^\dagger$.

In addition the MSSM contains a large number of parameters that parametrize soft SUSY breaking. Except where explicitly stated we will restrict the number of these parameters by neglecting generation mixing in the sfermion sectors. Furthermore, we restrict ourselves to the case of R -parity conservation, since R -parity violating interactions have not much impact on a_μ .

The SUSY particles of particular importance to a_μ are the smuons, muon-sneutrino, gauginos and Higgsinos since they appear in the SUSY one-loop contributions. At higher order, also other sectors of the MSSM become relevant, most notably the third generation squarks and the Higgs sector. Since in the MSSM all particles of equal quantum numbers can mix and these mixings have an important influence on the a_μ -prediction, we briefly discuss the mixing of the individual sectors in the following.

The sfermions $\tilde{f}_{L,R}$ for each flavour can mix, and the mass matrices corresponding to the \tilde{f}_L, \tilde{f}_R basis read

$$M_{\tilde{f}}^2 = \begin{pmatrix} M_{LL}^2 & m_f X_f^* \\ m_f X_f & M_{RR}^2 \end{pmatrix}, \quad (13)$$

where

$$M_{LL}^2 = m_f^2 + m_{L,\tilde{f}}^2 + M_Z^2 \cos 2\beta (I_3^f - Q^f s_W^2), \quad (14)$$

$$M_{RR}^2 = m_f^2 + m_{R,\tilde{f}}^2 + M_Z^2 \cos 2\beta Q^f s_W^2, \quad (15)$$

$$X_f = A_f - \mu^* \{\cot \beta, \tan \beta\} \quad (16)$$

with $\{\cot \beta, \tan \beta\}$ for up- and down-type sfermions, respectively. m_f , I_3^f and Q^f denote the mass, weak isospin and electric charge of the corresponding fermion; $s_W^2 \equiv \sin^2 \theta_W = 1 - M_W^2/M_Z^2$, where θ_W denotes the weak mixing angle and $M_{W,Z}$ the W and Z boson masses. The quantities A_f are soft SUSY breaking parameters

for trilinear interactions of sfermions with Higgs bosons of the form $\tilde{f}_L\text{-}\tilde{f}_R\text{-Higgs}$. The remaining entries $m_{L,R}$ of the diagonal elements are governed by the five independent soft SUSY-breaking parameters for each generation:

$$m_{L,\tilde{t}} = m_{L,\tilde{b}} \equiv M_{Q3}, \quad m_{R,\tilde{b}} \equiv M_{D3}, \quad m_{R,\tilde{t}} \equiv M_{U3}, \quad (17)$$

$$m_{L,\tilde{\mu}} = m_{L,\tilde{\nu}_\mu} \equiv M_{L2}, \quad m_{R,\tilde{\mu}} \equiv M_{R2}. \quad (18)$$

We have given these relations for 3rd generation squarks and 2nd generation sleptons as these are most important for our purposes. Analogous formulas hold for the other generations. The mass matrices can be diagonalized by unitary matrices $U^{\tilde{f}}$ in the form

$$U^{\tilde{f}} M_{\tilde{f}}^2 U^{\tilde{f}\dagger} = \text{diag}(m_{\tilde{f}_1}^2, m_{\tilde{f}_2}^2), \quad (19)$$

and sfermion mass eigenstates can be defined by

$$\begin{pmatrix} \tilde{f}_1 \\ \tilde{f}_2 \end{pmatrix} = U^{\tilde{f}} \begin{pmatrix} \tilde{f}_L \\ \tilde{f}_R \end{pmatrix}. \quad (20)$$

The mass of the sneutrino $\tilde{\nu}_\mu$ is given by

$$m_{\tilde{\nu}_\mu}^2 = m_{L,\tilde{\mu}}^2 + \frac{1}{2} M_Z^2 \cos 2\beta \quad (21)$$

and similar for the other generations.

The superpartners of the charged gauge and Higgs bosons also mix, and the mass and mixing terms can be easiest expressed in terms of the Weyl spinor combinations $\psi^- = (\tilde{W}^-, \tilde{H}_1^-)$, $\psi^+ = (\tilde{W}^+, \tilde{H}_2^+)$. The mass term for these fields is given by $\psi^- X \psi^+ + h.c.$ with the mass matrix

$$X = \begin{pmatrix} M_2 & M_W \sqrt{2} \sin \beta \\ M_W \sqrt{2} \cos \beta & \mu \end{pmatrix}, \quad (22)$$

where M_2 is the soft SUSY breaking parameter corresponding to the SU(2) gaugino mass. This matrix can be diagonalized using two unitary matrices U, V in the form

$$U^* X V^{-1} = \text{diag}(m_{\chi_1^\pm}, m_{\chi_2^\pm}). \quad (23)$$

Similarly, the mass matrix Y corresponding to the superpartners of the neutral gauge and Higgs bosons in the basis $\psi^0 = (\tilde{B}, \tilde{W}^3, \tilde{H}_1^0, \tilde{H}_2^0)$ is given by

$$Y = \begin{pmatrix} M_1 & 0 & -M_Z s_W \cos \beta & M_Z s_W \sin \beta \\ 0 & M_2 & M_Z c_W \cos \beta & -M_Z c_W \sin \beta \\ -M_Z s_W \cos \beta & M_Z c_W \cos \beta & 0 & -\mu \\ M_Z s_W \sin \beta & -M_Z c_W \sin \beta & -\mu & 0 \end{pmatrix}, \quad (24)$$

where M_1 is a U(1) gaugino (bino) soft SUSY breaking parameter and $c_W = M_W/M_Z$. It can be diagonalized with the help of one unitary matrix N in the form

$$N^* Y N^{-1} = \text{diag}(m_{\chi_1^0}, \dots, m_{\chi_4^0}). \quad (25)$$

The mass eigenstates corresponding to the charged and neutral gauginos and Higgsinos are called charginos and neutralinos, and they are related to the interaction eigenstates

by

$$\chi_i^+ = V_{ij}\psi_j^+, \quad (26)$$

$$\chi_i^- = U_{ij}\psi_j^-, \quad (27)$$

$$\chi_i^0 = N_{ij}\psi_j^0. \quad (28)$$

The gluinos do not mix, and their tree-level mass is given by $|M_3|$ in terms of the SU(3) gaugino mass parameter M_3 .

The SUSY parameters μ , A_f , $M_{1,2,3}$ can be complex. However, not all complex phases can appear in observables. The only physical phases of the MSSM (beyond the phase in the CKM matrix) are the ones of the combinations

$$\mu A_f, \quad \mu M_{1,2,3}. \quad (29)$$

Hence the frequently adopted convention that M_2 is real and positive constitutes no restriction. Below, we will adopt this convention only in section 4 and remain general elsewhere.

After spontaneous symmetry breaking the two MSSM Higgs doublets lead to 5 physical Higgs bosons and 3 unphysical Goldstone bosons. Parametrizing the two doublets in the form

$$\mathcal{H}_1 = \begin{pmatrix} v_1 + \frac{1}{\sqrt{2}}(\phi_1^0 - i\chi_1^0) \\ -\phi_1^- \end{pmatrix}, \quad \mathcal{H}_2 = \begin{pmatrix} \phi_2^+ \\ v_2 + \frac{1}{\sqrt{2}}(\phi_2^0 + i\chi_2^0) \end{pmatrix}, \quad (30)$$

the mass eigenstates are given by

$$\begin{pmatrix} H^0 \\ h^0 \end{pmatrix} = \begin{pmatrix} \cos \alpha & \sin \alpha \\ -\sin \alpha & \cos \alpha \end{pmatrix} \begin{pmatrix} \phi_1^0 \\ \phi_2^0 \end{pmatrix}, \quad (31)$$

$$\begin{pmatrix} G^0 \\ A^0 \end{pmatrix} = \begin{pmatrix} \cos \beta & \sin \beta \\ -\sin \beta & \cos \beta \end{pmatrix} \begin{pmatrix} \chi_1^0 \\ \chi_2^0 \end{pmatrix}, \quad (32)$$

$$\begin{pmatrix} G^\pm \\ H^\pm \end{pmatrix} = \begin{pmatrix} \cos \beta & \sin \beta \\ -\sin \beta & \cos \beta \end{pmatrix} \begin{pmatrix} \phi_1^\pm \\ \phi_2^\pm \end{pmatrix}, \quad (33)$$

where the mixing angle α is related to β and the mass M_A of the CP-odd scalar A^0 by

$$\tan 2\alpha = \tan 2\beta \frac{M_A^2 + M_Z^2}{M_A^2 - M_Z^2}, \quad -\frac{\pi}{2} < \alpha < 0. \quad (34)$$

The physical Higgs degrees of freedom are the light and heavy CP-even scalars h^0 , H^0 , the CP-odd scalar A^0 and the charged Higgs bosons H^\pm . For $M_A \gg M_Z$ the masses of H^0 and H^\pm are of the order M_A . The three unphysical Goldstone bosons $G^{0,\pm}$ are eaten to give masses to the Z and W^\pm bosons.

For the discussion of two-loop contributions to a_μ with Higgs exchange it is important to note that the muon receives its mass from the doublet \mathcal{H}_1 . In the case that $M_A \gg M_Z$ and $\tan \beta$ is large the heavy Higgs bosons H^0 , A^0 and H^\pm are predominantly composed of \mathcal{H}_1 -components. In this case they have larger couplings to the muon than the light Higgs boson h^0 .

1.3. Magnetic moment of the muon and chirality flips

The magnetic moment is a property of the muon in presence of an electromagnetic field. In quantum field theory it is related to the muon–photon vertex function $\Gamma_{\mu\bar{\mu}A\rho}(p, -p', q)$, which has the covariant decomposition

$$\bar{u}(p')\Gamma_{\mu\bar{\mu}A\rho}(p, -p', q)u(p) = e \bar{u}(p') \left[\gamma_\rho F_V(q^2) + (p + p')_\rho F_M(q^2) + \dots \right] u(p) \quad (35)$$

for on-shell momenta p, p' and spinors u, \bar{u} that satisfy the Dirac equation. The charge renormalization condition implies $F_V(0) + 2m_\mu F_M(0) = 1$, and rearranging (35) leads to a term

$$\frac{ie}{2m_\mu} [1 - 2m_\mu F_M(0)] \sigma_{\rho\nu} q^\nu \quad (36)$$

for $q^2 \rightarrow 0$ in the covariant decomposition. This term describes the interaction of the muon dipole moment with a magnetic field, and the corresponding gyromagnetic ratio is given by $g = 2[1 - 2m_\mu F_M(0)]$, or equivalently

$$a_\mu = -2m_\mu F_M(0). \quad (37)$$

In practical calculations it is often useful to extract the form factor F_M before evaluating the full vertex function with the help of projection operators [29, 30].

It is important to understand where the generic behaviour $a_\mu^{\text{SUSY}} \propto m_\mu^2/M_{\text{SUSY}}^2$ comes from and how it can be modified by additional factors.† The $1/M_{\text{SUSY}}^2$ -behaviour for SUSY masses of order M_{SUSY} reflects the decoupling properties of SUSY. The m_μ^2 -behaviour of a_μ , or equivalently the relation $F_M \propto m_\mu$ is related to chiral symmetry, and crucial modifications by additional factors are possible. The form factor F_M in (35) corresponds to a chirality-flipping interaction between the left- and right-handed muon. If the MSSM were invariant under the discrete chiral transformation

$$\left. \begin{array}{c} \left(\begin{array}{c} \nu_\mu \\ \mu_L \end{array} \right), \quad \left(\begin{array}{c} \tilde{\nu}_\mu \\ \tilde{\mu}_L \end{array} \right) \\ \mu_R, \quad \tilde{\mu}_R \end{array} \right\} \rightarrow \left\{ \begin{array}{cc} + \left(\begin{array}{c} \nu_\mu \\ \mu_L \end{array} \right), & + \left(\begin{array}{c} \tilde{\nu}_\mu \\ \tilde{\mu}_L \end{array} \right), \\ - \mu_R, & - \tilde{\mu}_R \end{array} \right. \quad (38)$$

of the left-handed doublets and right-handed singlets, F_M and thus a_μ would vanish in the MSSM. F_M is proportional to m_μ because the invariance of the MSSM under (38) is broken by the muon mass, or more precisely by all terms in the MSSM Lagrangian that are proportional to the muon Yukawa coupling. In each Feynman diagram that contributes to a_μ , the μ -chirality has to be flipped by one of these terms. The main possibilities for the chirality flip are illustrated in figure 1 and are the following:

- at a μ -line through a muon mass term, contributing a factor m_μ ,
- at a Yukawa coupling of \mathcal{H}_1 to μ_R and μ_L or ν_μ , contributing a factor y_μ ,
- at a $\tilde{\mu}$ -line, corresponding to the transition $\tilde{\mu}_L - \tilde{\mu}_R$, contributing a factor $m_\mu X_\mu \approx m_\mu \tan \beta$ for large $\tan \beta$ from the smuon mass matrix,
- at a SUSY Yukawa coupling of a Higgsino to μ and $\tilde{\mu}$ or $\tilde{\nu}_\mu$, contributing a factor y_μ .

† Logarithmic factors like $\log M_{\text{SUSY}}/m_\mu$, which can appear at the two-loop level, are disregarded here.

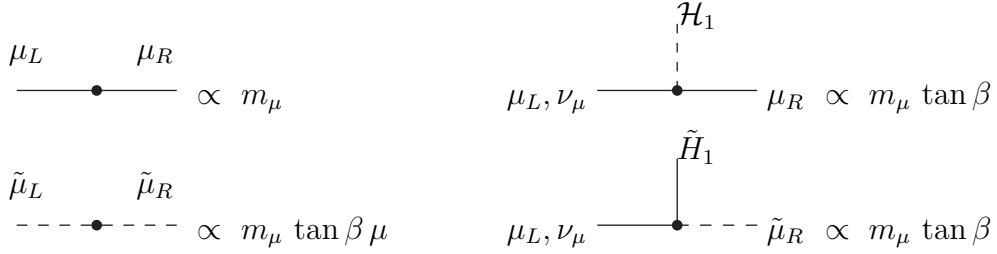


Figure 1. Possibilities for chirality-flips along the line carrying the μ -lepton number.

The muon Yukawa coupling y_μ is given by

$$y_\mu = \frac{m_\mu}{v_1} = \frac{m_\mu g_2}{\sqrt{2} M_W \cos \beta}, \quad (39)$$

where $g_2 = e/s_W$, and is thus enhanced by the factor $1/\cos \beta \approx \tan \beta$ for large $\tan \beta$ compared to its SM value. Hence, while all four possibilities are proportional to the muon mass m_μ , the last three are enhanced by a factor $\tan \beta$ for large $\tan \beta$. SUSY contributions to a_μ that make use of these enhanced chirality flips are themselves enhanced compared to the generic estimate $m_\mu^2/M_{\text{SUSY}}^2$.

2. Analytic results

In a theory with unbroken SUSY, the gyromagnetic ratio of a charged fermion is exactly 2 and thus $a_\mu = 0$ [31, 32], that is the SUSY contribution exactly cancels the SM contribution. In the MSSM, SUSY is softly broken, and SUSY contributions to a_μ were studied already in the early 1980's [33–39], when it was still conceivable that SUSY particles were significantly lighter than the W and Z bosons. Although very light SUSY particles are now experimentally excluded and SUSY contributions to a_μ are suppressed as $1/M_{\text{SUSY}}^2$, it is still possible that these contributions are significant. In the following we first discuss the generic size of the SUSY one- and two-loop contributions on a more intuitive level; then we present the analytic results for the most important contributions.

2.1. How large can the SUSY contributions be?

Before presenting the full SUSY one-loop contributions to a_μ [33–44], it is instructive to discuss the dominant parameter dependence on an intuitive level and to obtain useful estimates. As shown in section 1.3 the contributions from SUSY particles of a generic mass M_{SUSY} are of the order $m_\mu^2/M_{\text{SUSY}}^2$, and hence suppressed by a factor M_W^2/M_{SUSY}^2 compared to the SM electroweak contributions.

However, it has been observed in [37] and further stressed and discussed in [42–44] that the SUSY contributions can be significantly enhanced if $\tan \beta$ is large. Moreover, for large $\tan \beta$ the sign of the one-loop contributions is mainly determined by the sign of the μ -parameter introduced in (12). We will see here that not only the one-loop but also the leading two-loop contributions behave in this way.

(C)

$$\propto m_\mu^2 \tan \beta \mu M_2 F(\mu, M_2, m_{\tilde{\mu}_L})$$

(N1)

$$\propto m_\mu^2 \tan \beta \mu M_1 F(M_1, m_{\tilde{\mu}_{L,R}})$$

(N2)

$$\propto m_\mu^2 \tan \beta \mu M_1 F(\mu, M_1, m_{\tilde{\mu}_R})$$

(C_{2L})

$$\propto m_\mu^2 \tan \beta \mu M_2 F(\mu, M_2, M_{\mathcal{H}_1})$$

(\tilde{t}_{2L})

$$\propto m_\mu^2 \tan \beta \frac{\mu m_t}{M_W^2} (m_t X_t) F(m_{\tilde{t}_{L,R}}, M_{\mathcal{H}_1^0})$$

Figure 2. Five sample mass-insertion diagrams. Vertices and mass insertions are denoted by dots, and the interaction eigenstates corresponding to each line are displayed explicitly. The external photon has to be attached in all possible ways to the charged internal lines. The one-loop diagrams (C), (N1), (N2) have been discussed also in [44]. The loop functions F in the results are different in the five cases and depend on different masses.

It is easiest to understand the leading behaviour with the help of diagrams that are written in terms of interaction eigenstates, where the insertions of mass and mixing terms and chirality flips are explicitly shown [44]. The five diagrams in figure 2 exemplify the main enhancement mechanisms. The basic reason for the $\tan\beta$ -enhancement is the fact that the muon Yukawa coupling in the MSSM is larger by a factor $1/\cos\beta \approx \tan\beta$ for large $\tan\beta$ than its SM counterpart. This Yukawa coupling enters the diagrams in figure 2 in the vertices where the muon chirality is flipped, i.e. in the couplings of the muon to the Higgsino or Higgs boson in cases (C,N2,C_{2L}, \tilde{t}_{2L}), and in the $\tilde{\mu}_L$ - $\tilde{\mu}_R$ transition, given by $(M_\mu^2)_{12}$, in case (N1).

The second important parameter entering all five diagrams is the μ -parameter, which governs the mixing between the two Higgs doublets. In all cases, the enhancement due to this mixing can be traced back to the fact that \mathcal{H}_2 has the larger vacuum expectation value and strongly couples to top quarks, while only \mathcal{H}_1 couples to muons.

In diagrams (C,N2,C_{2L}) the μ -parameter enters via the Higgsino \tilde{H}_1 - \tilde{H}_2 transitions. These transitions enhance the diagrams because the following \tilde{H}_2 -gaugino transitions are by a factor $v_2 : v_1 = \tan\beta$ larger than \tilde{H}_1 -gaugino transitions. In diagram (N1) μ enters via the dominant part of the smuon mixing. This mass insertion is obtained from the F -term $F_{H_1}\mathcal{H}_2$, see (12), by replacing \mathcal{H}_2 by its large vacuum expectation value. Finally, in diagram (\tilde{t}_{2L}) the dominant part of the Higgs-stop coupling originates from $F_{H_2}\mathcal{H}_1$ and thus enables \mathcal{H}_1 to couple with the top-Yukawa coupling.

The remaining mass insertions in the diagrams provide additional factors of the gaugino mass $M_{1,2}$ and stop mixing parameter X_t . They are necessary in order to obtain an even number of γ -matrices in the fermion line and in order to connect \tilde{t}_L and \tilde{t}_R , respectively. As an illustration, the relevant factors of diagram (C) are given by

$$y_\mu X_{22} X_{12} X_{22} = \frac{m_\mu}{v_1} \mu (g_2 v_2) M_2 = g_2 m_\mu \tan\beta \mu M_2. \quad (40)$$

Combining the enhancement factors of all diagrams leads to the estimates given in figure 2. They all have a similar form,

$$a_\mu^{(C,C_{2L};N1,N2)} \propto m_\mu^2 \tan\beta \mu M_{2;1} F, \quad (41)$$

$$a_\mu^{(\tilde{t}_{2L})} \propto m_\mu^2 \tan\beta \frac{\mu m_t}{M_W^2} (m_t X_t) F, \quad (42)$$

where $M_{2;1}$ corresponds to (C, C_{2L}) and (N1, N2), respectively. The loop functions F are different in the five cases, depend on the masses appearing in the respective diagrams and generally behave as $F \propto M_{\text{SUSY}}^{-4}$ for large SUSY masses. In these formulas one power of m_μ is due to the a_μ - F_M relation (37) and gauge couplings have been suppressed.

Therefore all leading one- and two-loop contributions are approximately linear in $\tan\beta$, and their sign is given by the sign of μ , together with the sign of $M_{1,2}$ or X_t . Generally, all diagrams are suppressed by two powers of the SUSY mass scale. Hence the basic behaviour of diagrams (C,C_{2L},N1,N2) is given by

$$a_\mu^{(C,C_{2L};N1,N2)} \propto \frac{m_\mu^2}{M_{\text{SUSY}}^2} \tan\beta \text{sign}(\mu M_{2;1}) \quad (43)$$

if all SUSY masses are set equal to a common scale M_{SUSY} . However, it is important to keep in mind that the relevant SUSY masses are different in the five diagrams.

In particular, diagrams (N1) and (\tilde{t}_{2L}) are special because they increase linearly with μ , while the all other diagrams are suppressed for large μ by their μ -dependent loop functions F . Likewise, only the one-loop diagrams are sensitive to the smuon and sneutrino masses. If these are large, the one-loop diagrams can be suppressed and the two-loop diagrams can become dominant. The chargino-loop diagram (C_{2L}) can be large if the chargino and Higgs masses are small.

The discussion of the stop-loop diagram (\tilde{t}_{2L}) is complicated by the fact that the seemingly linear dependence on $(m_t X_t)$ is cut off by the requirement that both stop mass eigenvalues are positive. This diagram is largest for maximal stop mixing, i.e. if $(m_t X_t)$ is large but both eigenvalues are positive and $m_{\tilde{t}_1} \ll m_{\tilde{t}_2}$, and if $m_{\tilde{t}_1}$ and the Higgs boson mass are small. In this case, diagram (\tilde{t}_{2L}) has the behaviour

$$a_{\mu}^{(\tilde{t}_{2L})} \propto \frac{m_{\mu}^2}{M_{\text{SUSY}}^2} \frac{\mu m_t}{M_W^2} \tan \beta \text{sign}(X_t), \quad (44)$$

where M_{SUSY} denotes here the common mass scale of the appearing Higgs boson and the lightest stop. Thus the diagram is linearly enhanced by large μ , and its sign is determined by $\text{sign}(X_t)$. In the following subsections we will provide the exact analytical formulas for all these diagrams and also derive the numerical prefactors in the proportionalities (43) and (44).

2.2. One-loop contributions

Each diagram that contributes to a_{μ} contains one line carrying the μ -lepton number. This fact allows to divide the MSSM one-loop diagrams into two classes:

- (a) SM-like diagrams, where the μ -lepton number is carried only by μ and/or ν_{μ} .
- (b) SUSY diagrams, where the μ -lepton number is carried also by $\tilde{\mu}$ and/or $\tilde{\nu}_{\mu}$.

The diagrams of the first class involve only SM-particles, and they are essentially identical in the SM and the MSSM. The only non-identical diagrams involve two couplings of physical SM or MSSM Higgs bosons to the muon line. Owing to the additional suppression factor m_{μ}^2/M_W^2 such diagrams are entirely negligible both in the SM and the MSSM.

Therefore the SUSY one-loop contribution, i.e. the difference between a_{μ} in the MSSM and the SM, is given entirely by the diagrams of the second class. They are displayed in figure 3 and involve either a chargino–sneutrino or a neutralino–smuon loop. In contrast to the diagrams in figure 2 they are written in terms of interaction eigenstates, which is more appropriate for an exact evaluation. The diagrams have been evaluated in Refs. [33–36] with various restrictions on the masses and mixings. These restrictions have been dropped in Refs. [37–40], and exact results have been derived. Later, more comprehensive and general evaluations of these diagrams have been presented in the context of particular supersymmetric models [41–43] and the

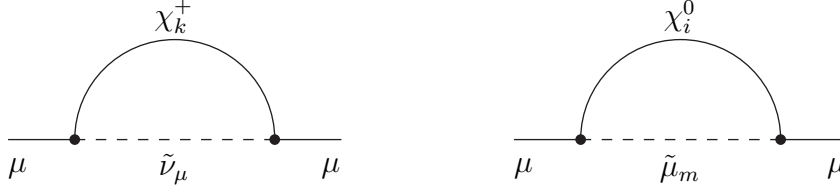


Figure 3. The two SUSY one-loop diagrams, written in terms of mass eigenstates. The external photon line has to be attached to the charged internal lines.

unconstrained MSSM [44] (see also [45, 46] for related results on weak dipole moments in the MSSM). We present the general result in the form given in [47]:

$$a_\mu^{\text{SUSY,1L}} = a_\mu^{\chi^0} + a_\mu^{\chi^\pm}, \quad (45)$$

with

$$a_\mu^{\chi^0} = \frac{m_\mu}{16\pi^2} \sum_{i,m} \left\{ -\frac{m_\mu}{12m_{\tilde{\mu}_m}^2} (|n_{im}^L|^2 + |n_{im}^R|^2) F_1^N(x_{im}) + \frac{m_{\chi_i^0}}{3m_{\tilde{\mu}_m}^2} \text{Re}[n_{im}^L n_{im}^R] F_2^N(x_{im}) \right\}, \quad (46)$$

$$a_\mu^{\chi^\pm} = \frac{m_\mu}{16\pi^2} \sum_k \left\{ \frac{m_\mu}{12m_{\tilde{\nu}_\mu}^2} (|c_k^L|^2 + |c_k^R|^2) F_1^C(x_k) + \frac{2m_{\chi_k^\pm}}{3m_{\tilde{\nu}_\mu}^2} \text{Re}[c_k^L c_k^R] F_2^C(x_k) \right\}, \quad (47)$$

where $i = 1 \dots 4$ and $k = 1, 2$ denote the neutralino and chargino indices, $m = 1, 2$ denotes the smuon index, and the couplings are given by

$$n_{im}^L = \frac{1}{\sqrt{2}} (g_1 N_{i1} + g_2 N_{i2}) U_{m1}^{\tilde{\mu}*} - y_\mu N_{i3} U_{m2}^{\tilde{\mu}*}, \quad (48)$$

$$n_{im}^R = \sqrt{2} g_1 N_{i1} U_{m2}^{\tilde{\mu}} + y_\mu N_{i3} U_{m1}^{\tilde{\mu}}, \quad (49)$$

$$c_k^L = -g_2 V_{k1}, \quad (50)$$

$$c_k^R = y_\mu U_{k2}. \quad (51)$$

The kinematic variables are defined as the mass ratios $x_{im} = m_{\chi_i^0}^2/m_{\tilde{\mu}_m}^2$, $x_k = m_{\chi_k^\pm}^2/m_{\tilde{\nu}_\mu}^2$, and the loop functions are given by

$$F_1^N(x) = \frac{2}{(1-x)^4} [1 - 6x + 3x^2 + 2x^3 - 6x^2 \log x], \quad (52)$$

$$F_2^N(x) = \frac{3}{(1-x)^3} [1 - x^2 + 2x \log x], \quad (53)$$

$$F_1^C(x) = \frac{2}{(1-x)^4} [2 + 3x - 6x^2 + x^3 + 6x \log x], \quad (54)$$

$$F_2^C(x) = \frac{3}{(1-x)^3} [-3 + 4x - x^2 - 2 \log x], \quad (55)$$

normalized such that $F_i^j(1) = 1$. The U(1) and SU(2) gauge couplings are given by $g_{1,2} = e/\{c_W, s_W\}$, such that the one-loop contributions are of the order $\alpha = e^2/(4\pi)$. A class of large two-loop logarithms can be taken into account by the replacement $\alpha \rightarrow \alpha(M_{\text{SUSY}})$ (see later for more details).

For discussing the one-loop contributions $a_\mu^{\chi^{0,\pm}}$ it is noteworthy that the terms linear in $m_{\chi^{0,\pm}}$ are not enhanced by a factor $m_{\chi^{0,\pm}}/m_\mu$ compared to the other terms. Rather,

these terms involve either an explicit factor of the muon Yukawa coupling y_μ or of the combination $U_{m1}^\mu U_{m2}^\mu / m_{\tilde{\mu}m}^2$, which in turn is proportional to $(M_\mu^2)_{12}$ and thus to y_μ . Hence, all terms are of the same basic order $m_\mu^2 / M_{\text{SUSY}}^2$, and the terms linear in $m_{\chi^{0,\pm}}$ are enhanced merely by a factor $\tan \beta$ from the muon Yukawa coupling.

It is instructive to close this subsection by deriving a simple approximation of (46), (47) for large $\tan \beta$ and the case that all SUSY mass parameters in the smuon, chargino and neutralino mass matrices are equal to a common scale M_{SUSY} . In this case only the terms linear in $m_{\chi^{0,\pm}}$ have to be considered, and the loop functions $F_i^j(x)$ can be approximated by a Taylor series around $x = 1$. For example, the factors $m_{\chi_k^\pm} c_k^L c_k^R F_2^C(x_k)$ appearing in $a_\mu^{\chi^\pm}$ can be approximated as

$$-g_2 y_\mu \sum_k U_{k2} V_{k1} m_{\chi_k^\pm} \left(\frac{7}{4} - \frac{3}{4} \frac{m_{\chi_k^\pm}^2}{m_{\tilde{\nu}_\mu}^2} \right) \approx \frac{3g_2 y_\mu}{4} \frac{X_{22}(X^\dagger)_{21} X_{11}}{m_{\tilde{\nu}_\mu}^2} \approx \frac{3g_2 y_\mu}{4} \text{sign}(\mu M_2) X_{12}. \quad (56)$$

Here terms that are suppressed by $1/\tan \beta$ or M_W/M_{SUSY} have been neglected. Note that the factors on the right-hand side correspond directly to the mass-insertion diagram (C) in figure 2 and the approximation (43). The factors appearing in $a_\mu^{\chi^0}$ can be similarly approximated. Inserting these approximations, one obtains [44]

$$a_\mu^{\chi^0} = \frac{g_1^2 - g_2^2}{192\pi^2} \frac{m_\mu^2}{M_{\text{SUSY}}^2} \text{sign}(\mu M_2) \tan \beta \left[1 + \mathcal{O}\left(\frac{1}{\tan \beta}, \frac{M_W}{M_{\text{SUSY}}}\right) \right], \quad (57)$$

$$a_\mu^{\chi^\pm} = \frac{g_2^2}{32\pi^2} \frac{m_\mu^2}{M_{\text{SUSY}}^2} \text{sign}(\mu M_2) \tan \beta \left[1 + \mathcal{O}\left(\frac{1}{\tan \beta}, \frac{M_W}{M_{\text{SUSY}}}\right) \right], \quad (58)$$

where real parameters and equal signs of M_1 and M_2 have been assumed.

2.3. Two-loop contributions

It is useful to classify the MSSM two-loop diagrams similar to the one-loop diagrams, into

- (a) two-loop corrections to SM one-loop diagrams, where the μ -lepton number is carried only by μ and/or ν_μ .
- (b) two-loop corrections to SUSY one-loop diagrams, where the μ -lepton number is carried also by $\tilde{\mu}$ and/or $\tilde{\nu}_\mu$.

The first class contains in particular SM-like diagrams with an insertion of a loop of SUSY particles, e.g. of \tilde{t} , \tilde{b} or χ^\pm . Such diagrams are particularly interesting since they constitute SUSY two-loop contributions that involve other particles and have a completely different parameter dependence than the SUSY one-loop contributions. Most importantly, these two-loop contributions can be large even if $a_\mu^{\text{SUSY,1L}}$ is suppressed. The contributions of this class are exactly known [48, 49].

The SUSY two-loop contributions of the second class involve the same particles as the SUSY one-loop contributions (possibly plus additional ones). Hence they can be expected to have a similar parameter dependence as $a_\mu^{\text{SUSY,1L}}$. The contributions of this class are known in the approximation of leading QED-logarithms [50].

2.3.1. *Two-loop corrections to SM one-loop diagrams* The MSSM two-loop contributions of the first class can be decomposed into a SM- and SUSY-part,

$$a_\mu^{\text{SM},2\text{L}} + a_\mu^{\text{SUSY},2\text{L(a)}}, \quad (59)$$

where $a_\mu^{\text{SM},2\text{L}}$ denotes the SM two-loop contributions. The genuine SUSY contributions of this class can be split into four parts:

$$a_\mu^{\text{SUSY},2\text{L(a)}} = a_\mu^{\chi,2\text{L}} + a_\mu^{\tilde{f},2\text{L}} + a_\mu^{\text{SUSY,ferm},2\text{L}} + a_\mu^{\text{SUSY,bos},2\text{L}}. \quad (60)$$

The first two terms correspond to diagrams involving a closed chargino/neutralino or sfermion loop, respectively. These diagrams are further categorized according to the particles coupling to the muon line,

$$a_\mu^{X,2\text{L}} = a_\mu^{(XVH)} + a_\mu^{(XVV)} + a_\mu^{(XVG)}, \quad X = \chi, \tilde{f}. \quad (61)$$

Diagrams where one gauge boson and one physical Higgs boson couple to the muon line are denoted as (XVH) with $V = \gamma, W, Z$ and $H = h^0, H^0, A^0, H^\pm$. Diagrams where only gauge bosons or unphysical Goldstone bosons couple to the muon are denoted as (XVV) , (XVG) .[‡] Sample diagrams are shown in figure 4.

The remaining two terms in (60) correspond to diagrams involving only SM- or two-Higgs-doublet model particles and no SUSY particles. These diagrams are different in the MSSM and the SM due to the additional Higgs bosons and the modified Higgs boson couplings. $a_\mu^{\text{SUSY,ferm},2\text{L}}$ denotes the difference between the MSSM- and SM-evaluation of the diagrams involving a SM fermion (i.e. quark or lepton) loop; likewise, $a_\mu^{\text{SUSY,bos},2\text{L}}$ denotes the corresponding difference of the diagrams without fermion loop, the so-called bosonic contributions. Sample diagrams are shown in figure 5.

The SUSY two-loop diagrams can be conveniently evaluated by first applying a large mass expansion [51], where the muon mass is treated as small and all other masses as large. This results in a separation of scales, and all remaining integrals are of one of two types. One type are one-scale two-point integrals with external momentum $p^2 = m_\mu^2$ and all internal masses being either zero or equal to m_μ . The other type are integrals where all internal masses are heavy but the external momentum can be neglected. All these integrals and the corresponding prefactors can be evaluated analytically [48, 49]. In addition to the genuine two-loop diagrams, one-loop counterterm diagrams have to be evaluated. These contain renormalization constants corresponding to charge, mass, and tadpole renormalization, which are defined in the on-shell renormalization scheme [26, 52, 53].

The diagrams of classes (XVH) , $X = \chi, \tilde{f}, f$ can be calculated in an alternative way. In these so-called Barr-Zee diagrams [54], a closed loop generates an effective γ - V - H vertex, and this vertex can be evaluated first by a one-loop computation. By inserting the result and performing the second loop integral one obtains a simple integral representation for the full two-loop diagram. Barr-Zee diagrams were first considered because they give rise to important contributions to electric dipole moments

[‡] Diagrams of the form (XHH) , (XHG) etc. in which two Higgs or Goldstone bosons couple to the muon line are suppressed by an additional muon Yukawa coupling and can be neglected.

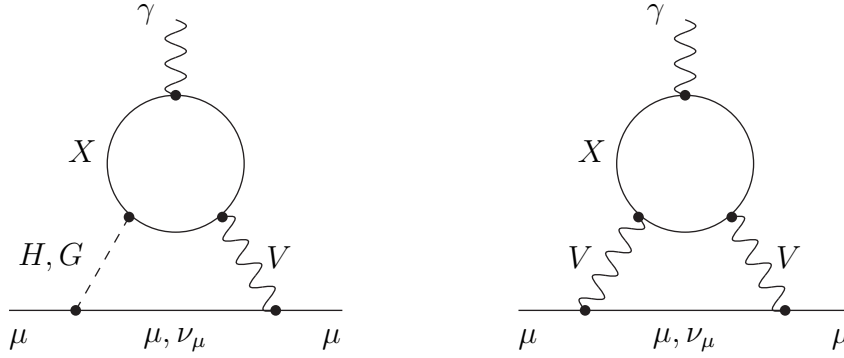


Figure 4. Sample two-loop diagrams with closed chargino/neutralino or sfermion loop, contributing to $a_\mu^{X,2L}$ and $a_\mu^{\tilde{f},2L}$. The diagrams are categorized into classes (XVH) , (XVG) and (XVV) , where $X = \chi^{\pm,0}, \tilde{f}$. $V = \gamma, Z, W^\pm$ denotes gauge bosons, $H = h^0, H^0, A^0, H^\pm$ denotes physical Higgs bosons, and $G = G^{\pm,0}$ denotes Goldstone bosons. See [48, 49] for more details on the possible diagram topologies.

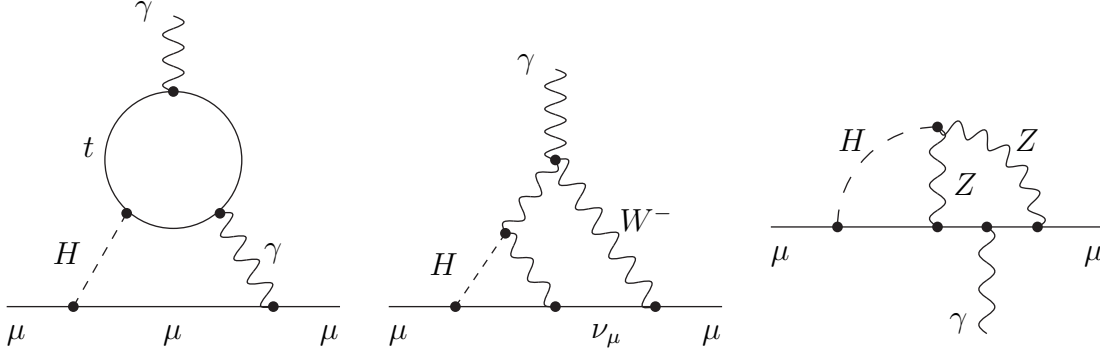


Figure 5. Sample two-loop diagrams involving only SM- or two-Higgs-doublet model particles and either with or without fermion loop. These diagrams are different in the MSSM and the SM due to the modified Higgs sector, and this difference constitutes the SUSY contributions $a_\mu^{\text{SUSY,ferm},2L}$ and $a_\mu^{\text{SUSY,bos},2L}$.

in extensions of the SM (see e.g. Refs. [54–56]). The contributions from particular Barr-Zee diagrams of the classes $(f\gamma A^0)$, $(f\gamma H)$, $(\tilde{f}\gamma H)$, $(\tilde{f}W^\pm H^\mp)$ to a_μ were considered in Refs. [57–60], respectively.

In Refs. [48, 49] the numerical results of all two-loop contributions in (60) were compared and analyzed in detail, taking into account that the SUSY parameters are constrained by experimental bounds on b -decays, M_h and other quantities. It turned out that the numerical values of the various contributions is very different:

- The by far largest contributions are the ones from the photonic Barr-Zee diagrams $(\chi\gamma H)$ and $(\tilde{f}\gamma H)$, where H denotes the neutral physical Higgs bosons h^0, H^0, A^0 . As explained in section 2.1 they are enhanced by a factor $\tan\beta$ and, in the case of the sfermion loop diagrams, by the potentially large Higgs–sfermion coupling. They can have values up to

$$a_\mu^{(\chi\gamma H)}, a_\mu^{(\tilde{f}\gamma H)} \sim \mathcal{O}(10) \times 10^{-10}. \quad (62)$$

Barr-Zee diagrams with Z or W^\pm exchange have a similar parameter dependence but are typically smaller by a factor of about 3–5.

- The diagrams of classes (χVV) and $(\tilde{f}VV)$ and the corresponding Goldstone diagrams (χVG) and $(\tilde{f}VG)$ involve no enhanced muon–Higgs Yukawa coupling and thus no $\tan\beta$ -enhancement, and they do not involve any other enhancement factors. Their numerical impact is tiny. For SUSY masses larger than 100 GeV these contributions are smaller than 0.1×10^{-10} .
- The genuine SUSY contributions to the SM-like diagrams $a_\mu^{\text{SUSY,ferm,2L}}$ and $a_\mu^{\text{SUSY,bos,2L}}$ depend only on $\tan\beta$ and M_A and are small. Only for $M_A < 200$ GeV they can reach 10^{-10} , but for larger M_A they are typically below 0.5×10^{-10} .

Hence, for the purpose of the present review, we only present the analytical result for the dominant contributions from the photonic Barr-Zee diagrams with physical Higgs bosons. They can be written as

$$a_\mu^{(\chi\gamma H)} = \frac{\alpha^2 m_\mu^2}{8\pi^2 M_W^2 s_W^2} \sum_{k=1,2} \left[\text{Re}[\lambda_\mu^{A^0} \lambda_{\chi_k^+}^{A^0}] f_{PS}(m_{\chi_k^+}^2/M_{A^0}^2) + \sum_{S=h^0, H^0} \text{Re}[\lambda_\mu^S \lambda_{\chi_k^+}^S] f_S(m_{\chi_k^+}^2/M_S^2) \right], \quad (63)$$

$$a_\mu^{(\tilde{f}\gamma H)} = \frac{\alpha^2 m_\mu^2}{8\pi^2 M_W^2 s_W^2} \sum_{\tilde{f}=\tilde{t}, \tilde{b}, \tilde{\tau}} \sum_{i=1,2} \left[\sum_{S=h^0, H^0} (N_c Q^2)_{\tilde{f}} \text{Re}[\lambda_\mu^S \lambda_{\tilde{f}_i}^S] f_{\tilde{f}}(m_{\tilde{f}_i}^2/M_S^2) \right]. \quad (64)$$

The Higgs–muon and Higgs–chargino coupling factors are given by

$$\lambda_\mu^{\{h^0, H^0, A^0\}} = \left\{ -\frac{s_\alpha}{c_\beta}, \frac{c_\alpha}{c_\beta}, t_\beta \right\}, \quad (65)$$

$$\lambda_{\chi_k^+}^{\{h^0, H^0, A^0\}} = \frac{\sqrt{2} M_W}{m_{\chi_k^+}} (U_{k1} V_{k2} \{c_\alpha, s_\alpha, -c_\beta\} + U_{k2} V_{k1} \{-s_\alpha, c_\alpha, -s_\beta\}). \quad (66)$$

In the Higgs–sfermion couplings we neglect terms that are subleading in $\tan\beta$ and that give rise to negligible contributions to a_μ :

$$\lambda_{\tilde{t}_i}^{\{h^0, H^0\}} = \frac{2m_t}{m_{\tilde{t}_i}^2 s_\beta} (+\mu^* \{s_\alpha, -c_\alpha\} + A_t \{c_\alpha, s_\alpha\}) (U_{i1}^{\tilde{t}})^* U_{i2}^{\tilde{t}}, \quad (67)$$

$$\lambda_{\tilde{b}_i}^{\{h^0, H^0\}} = \frac{2m_b}{m_{\tilde{b}_i}^2 c_\beta} (-\mu^* \{c_\alpha, s_\alpha\} + A_b \{-s_\alpha, c_\alpha\}) (U_{i1}^{\tilde{b}})^* U_{i2}^{\tilde{b}}, \quad (68)$$

$$\lambda_{\tilde{\tau}_i}^{\{h^0, H^0\}} = \frac{2m_\tau}{m_{\tilde{\tau}_i}^2 c_\beta} (-\mu^* \{c_\alpha, s_\alpha\} + A_\tau \{-s_\alpha, c_\alpha\}) (U_{i1}^{\tilde{\tau}})^* U_{i2}^{\tilde{\tau}}. \quad (69)$$

The loop integral function f_{PS} can be given either as a one-dimensional integral or in terms of dilogarithms:

$$f_{PS}(z) = z \int_0^1 \frac{dx \log \frac{x(1-x)}{z}}{x(1-x) - z} = \frac{2z}{y} \left[\text{Li}_2\left(1 - \frac{1-y}{2z}\right) - \text{Li}_2\left(1 - \frac{1+y}{2z}\right) \right] \quad (70)$$

with $y = \sqrt{1-4z}$. Note that $f_{PS}(z)$ is real and analytic even for $z \geq 1/4$. The other loop functions are related to f_{PS} as

$$f_S(z) = (2z-1)f_{PS}(z) - 2z(2+\log z), \quad (71)$$

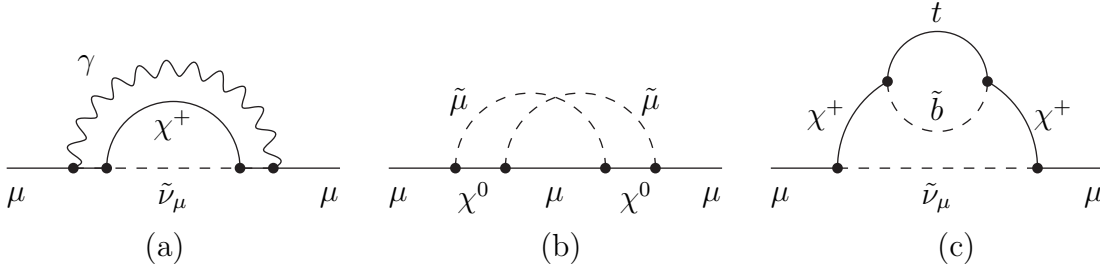


Figure 6. Sample two-loop diagrams contributing to $a_\mu^{\text{SUSY},2\text{L}(b)}$, i.e. involving a SUSY one-loop diagram. The external photon can be attached to all charged internal lines. (a) shows a diagram with additional photon loop, giving rise to large QED-logarithms. (b) shows a diagram of the class computed in [63]. (c) shows a diagram with an additional fermion/sfermion loop.

$$f_{\tilde{f}}(z) = \frac{z}{2} [2 + \log z - f_{PS}(z)]. \quad (72)$$

We remark that useful numerical estimates for the leading two-loop contributions can be obtained by taking into account only the $\tan\beta$ -enhanced terms in the couplings and by approximating the loop functions. In the case of the sfermion-loop contributions, simple approximations for the most important Barr-Zee diagrams ($\tilde{t}HV$), ($\tilde{b}HV$) with stop or sbottom loops can be derived [48]. The approximation for ($\tilde{t}HV$) agrees with the estimate (44) discussed in section 2.1, and the approximation for ($\tilde{b}HV$) has a similar form. In the case of the chargino/neutralino-loop diagrams the parameter dependence is simpler, and the diagrams with W - and Z -exchange can be included in the approximation [49]. We will collect all these approximations below in equations (81)–(83).

2.3.2. Two-loop corrections to SUSY one-loop diagrams The two-loop corrections to SUSY one-loop diagrams can be decomposed into two pieces,

$$a_\mu^{\text{SUSY},2\text{L}(b)} = c_L^{\text{SUSY},2\text{L}(b)} \log \frac{M_{\text{SUSY}}}{m_\mu} + c_0^{\text{SUSY},2\text{L}(b)}. \quad (73)$$

The first piece contains the large logarithm of the ratio M_{SUSY}/m_μ , where M_{SUSY} is the generic SUSY mass scale, and the second piece contains at most small logarithms of ratios of different SUSY masses. Sample diagrams are shown in figure 6. The diagrams all involve the same particles and the same couplings as the SUSY one-loop diagrams (possibly plus additional ones). Hence the overall parameter dependence of $a_\mu^{\text{SUSY},2\text{L}(b)}$ and of $a_\mu^{\text{SUSY},1\text{L}}$ can be expected to be similar, up to the additional two-loop suppression of $a_\mu^{\text{SUSY},2\text{L}(b)}$. The large logarithm is the most relevant enhancement factor.

The decomposition (73) is analogous to the one of the bosonic two-loop contributions in the SM, which have been evaluated in [49, 61, 62]. In the case of the SM, the term enhanced by $\log M_Z/m_\mu$ is roughly a factor 10 larger than the non-logarithmic piece.

In the case of the MSSM, the logarithmic term is known [50], but for the non-logarithmic remainder only a particular subclass of diagrams has been computed recently

[63]. In the following we first discuss the logarithmic term, which can be assumed to be dominant like in the SM, and then we describe the computation of [63].

The large logarithms in (73) are QED-logarithms and arise from two-loop diagrams that involve a SUSY one-loop diagram and an additional photon loop. The loop integrals of such diagrams have an infrared singularity in the limit $m_\mu \rightarrow 0$ and therefore give rise to terms $\propto \log m_\mu$. As shown by [50], the appropriate framework to evaluate these logarithms efficiently is the framework of effective field theories.

The relevant effective field theory is obtained from the MSSM by integrating out all fields of mass $\geq M_{\text{SUSY}}$ and retaining only the muon and photon. All further light or heavy SM fields are irrelevant in this analysis and can be ignored. The resulting theory is QED with additional higher-dimensional terms, described by

$$\mathcal{L}_{\text{eff}} = -2\sqrt{2}G_\mu \sum_i C_i(\mu) \mathcal{O}_i \quad (74)$$

in the notation of [50]. The \mathcal{O}_i are higher-dimensional operators. The analysis of [50] shows that in the MSSM, like in many new physics models, only one higher-dimensional operator has to be considered, namely the one corresponding to the muon anomalous magnetic moment,

$$H_\mu = -\frac{e}{16\pi^2} m_\mu \bar{\mu} \sigma^{\nu\rho} \mu F_{\nu\rho}. \quad (75)$$

The prefactors $C_i(\mu)$ are renormalization-scale dependent Wilson coefficients, which can be determined by matching the effective theory to the full MSSM at the high scale M_{SUSY} . Determining the Wilson coefficient $C_{H_\mu}(M_{\text{SUSY}})$ thus corresponds to the one-loop computation of a_μ^{SUSY} .

By construction, the large logarithms are identical in the full MSSM and the effective theory. However, in the effective theory the logarithms can be obtained simply from the one-loop renormalization-group running of the Wilson coefficient $C_{H_\mu}(\mu)$ from $\mu = M_{\text{SUSY}}$ down to $\mu = m_\mu$. This running is described by

$$C_{H_\mu}(\mu) = C_{H_\mu}(M_{\text{SUSY}}) - \gamma(H_\mu, H_\mu) \frac{\alpha(\mu)}{4\pi} \log \frac{M_{\text{SUSY}}}{\mu} C_{H_\mu}(M_{\text{SUSY}}). \quad (76)$$

where $\gamma(H_\mu, H_\mu)$ is the anomalous dimension of H_μ . On a diagrammatic level, the correspondence of this formula to the two-loop computation in the full MSSM is easy to see. In the MSSM, the logarithms arise from diagrams like the one in figure 6 (a). Corresponding diagrams in the effective theory are obtained by contracting the insertion of the SUSY one-loop diagram to a point. The resulting diagrams are one-loop contributions to H_μ , involving the effective vertex H_μ . Their UV-divergence, and thus their $\log \mu$ -terms, determine the anomalous dimension $\gamma(H_\mu, H_\mu)$.

The value of the anomalous dimension is

$$\gamma(H_\mu, H_\mu) = 16. \quad (77)$$

As a result, the QED-logarithms in the two-loop contributions to a_μ^{SUSY} are given by

$$a_\mu^{\text{SUSY},2\text{L}(b)} = -\frac{4\alpha}{\pi} \log \frac{M_{\text{SUSY}}}{m_\mu} a_\mu^{\text{SUSY},1\text{L}} + c_0^{\text{SUSY},2\text{L}(b)}. \quad (78)$$

This logarithmic correction is negative, and it amounts to $-7\% \dots -9\%$ of the SUSY one-loop contributions for M_{SUSY} between 100 and 1000 GeV. This result can be compared to the case of the bosonic SM two-loop contributions, where the logarithms amount to -19% of the SM electroweak one-loop result.

As mentioned before, the non-logarithmic terms in $a_\mu^{\text{SUSY},2\text{L}(b)}$, $c_0^{\text{SUSY},2\text{L}(b)}$, are not known so far. A first evaluation of a subclass of diagrams has been carried out in [63]. The considered diagrams involve only sleptons, charginos and neutralinos, and only topologies as in figure 6 (b) are taken into account that contain no self-energy subdiagrams. These diagrams constitute a finite contribution to $c_0^{\text{SUSY},2\text{L}(b)}$. However, the result of [63] can only be viewed as intermediate because there are more diagrams, e.g. containing self-energy subdiagrams or W - or Z -exchange, that would involve exactly the same coupling constants, such that non-trivial cancellations could be possible.

Nevertheless, the investigation of [63] provides a first insight to the possible values of the remaining two-loop contributions. The numerical values found in [63] are surprisingly large. In a range of SUSY parameters with SUSY masses of the order 300...500 GeV, the values are mostly below 10^{-10} but can become up to 2×10^{-10} , which is significantly larger than the corresponding non-logarithmic terms of the bosonic SM two-loop contributions.

2.4. Summary of known contributions and error estimate

To summarize, the SUSY contributions to a_μ up to the two-loop level, i.e. the difference of a_μ in the MSSM and the SM, are given by

$$\begin{aligned} a_\mu^{\text{SUSY}} = & a_\mu^{\text{SUSY},1\text{L}} \left(1 - \frac{4\alpha}{\pi} \log \frac{M_{\text{SUSY}}}{m_\mu} \right) + a_\mu^{(\chi\gamma H)} + a_\mu^{(\tilde{f}\gamma H)} \\ & + a_\mu^{(\chi\{W,Z\}H)} + a_\mu^{(\tilde{f}\{W,Z\}H)} + a_\mu^{\text{SUSY,ferm},2\text{L}} + a_\mu^{\text{SUSY,bos},2\text{L}} + \dots, \end{aligned} \quad (79)$$

where the terms in the first line have been given analytically in (45), (63), (64), (78). Note that the discussion of the two-loop QED-logarithms and equation (76) also show that the one-loop result should be parametrized in terms of the running $\alpha(M_{\text{SUSY}})$. In practice, it is sufficiently accurate to approximate $\alpha(M_{\text{SUSY}})$ by $\alpha(M_Z) = 1/127.9$, and we define M_{SUSY} in the logarithm as the mass of the lightest charged SUSY particle.

For many applications it should be sufficient to take into account the terms in the first line. The explicitly written terms in the second line are known, and they can be up to $\mathcal{O}(1) \times 10^{-10}$, but in the largest part of the MSSM parameter space they are much smaller. The dots denote the known but negligible contributions of the type (χVV) , $(\tilde{f} VV)$, the contributions evaluated in [63], and the remaining unknown two-loop contributions.

Handy approximations for the dominant terms are given by

$$a_\mu^{\text{SUSY},1\text{L}} \approx 13 \times 10^{-10} \left(\frac{100 \text{ GeV}}{M_{\text{SUSY}}} \right)^2 \tan \beta \text{ sign}(\mu M_2), \quad (80)$$

$$a_\mu^{(\chi V H)} \approx 11 \times 10^{-10} \left(\frac{\tan \beta}{50} \right) \left(\frac{100 \text{ GeV}}{M_{\text{SUSY}}} \right)^2 \text{ sign}(\mu M_2), \quad (81)$$

$$a_\mu^{(\tilde{t}\gamma H)} \approx -13 \times 10^{-10} \left(\frac{\tan \beta}{50} \right) \left(\frac{m_t}{m_{\tilde{t}}} \right) \left(\frac{\mu}{20M_H} \right) \text{sign}(X_t), \quad (82)$$

$$a_\mu^{(\tilde{b}\gamma H)} \approx -3.2 \times 10^{-10} \left(\frac{\tan \beta}{50} \right) \left(\frac{m_b \tan \beta}{m_{\tilde{b}}} \right) \left(\frac{A_b}{20M_H} \right) \text{sign}(\mu). \quad (83)$$

The first two are valid if all SUSY masses are approximately equal (note that the relevant masses are different in the two cases), and the third and fourth are valid if the stop/sbottom mixing is large and the relevant stop/sbottom and Higgs masses are of similar size. The result for the $(\tilde{b}\gamma H)$ contribution has not been here discussed before, but it can be understood in the same way as the $(\tilde{t}\gamma H)$ result [48].

In the following we list the missing contributions and estimate the theory error of the SUSY prediction (79).

- Two-loop QED-corrections beyond the leading logarithm (78). The leading-log approximation does not exactly fix the scale M_{SUSY} in the logarithm and in $\alpha(M_{\text{SUSY}})$ (the latter appears in the one-loop result). The exact form of the logarithms and of the non-logarithmic terms can only be found by a complete computation of the two-loop diagrams with a SUSY one-loop diagram and additional photon exchange. The error of the approximation (78) can be estimated by varying M_{SUSY} in the range 100...1000 GeV to about 2% of the SUSY one-loop contributions. If the SUSY contributions to a_μ are the origin of the observed deviation (5), they are certainly smaller than roughly 50×10^{-10} , and then this error is below 1×10^{-10} .
- Further electroweak and SUSY two-loop corrections to SUSY one-loop diagrams. These corrections include two-loop diagrams similar to figure 6 (a) but with W^- , Z^- , Higgs- instead of photon-exchange, and like in figure 6 (b) with purely SUSY particles in the loops. Given the result for the subclass evaluated in [63], we assign an error of $\pm 2 \times 10^{-10}$ to these diagrams. Note that this is a factor of 10 larger than the known result of the corresponding non-logarithmic bosonic two-loop contributions in the SM [49, 61, 62].
- Two-loop corrections to SUSY one-loop diagrams with fermion/sfermion-loops (see figure 6 (c) for an example). This class of diagrams involves in particular top/stop- and bottom/sbottom-loops, which are enhanced by the large 3rd generation Yukawa couplings. We estimate the numerical value of these diagrams to be less than $\pm 0.5 \times 10^{-10}$ for not too light SUSY masses for the following reasons. SUSY relates these diagrams to SM diagrams with top/bottom loops, which amount to about 0.6×10^{-10} but are not suppressed by possibly heavy SUSY masses. SUSY also relates the fermion/sfermion-loop diagrams to pure sfermion-loop diagrams such as $a_\mu^{(\tilde{f}\gamma H)}$, see (82), (83). However, this relation should be most accurate for rather small $A_{t,b}$ and μ , since the fermion/sfermion-loop diagrams are not enhanced by making these parameters large. In that case, the approximations (82), (83) lead to values below 0.5×10^{-10} .
- Three-loop contributions. In general, three-loop contributions can be expected to

be significantly smaller than the two-loop contributions. Two potential exceptions are three-loop diagrams that correspond to the two-loop contributions of the types $(\chi\gamma H)$, $(\tilde{f}\gamma H)$ with subloop-corrections to the Higgs-boson masses or the b -quark Yukawa coupling. It is well-known that the one-loop corrections to the Higgs-boson masses, in particular to M_h , and to y_b can be very large. Hence, in cases where the diagrams with h -exchange and/or sbottom loop are very large, the missing three-loop contributions could amount to $\mathcal{O}(1) \times 10^{-10}$. Fortunately, however, the influence of the lightest Higgs boson mass and y_b on the $(\chi\gamma H)$, $(\tilde{f}\gamma H)$ diagrams is small in the largest part of the MSSM parameter space. Hence we neglect the theory error associated with the missing three-loop contributions.

To summarize, we estimate the theory error associated with (79) to

$$\delta a_\mu^{\text{SUSY}}(\text{unknown}) = 0.02 a_\mu^{\text{SUSY,1L}} + 2.5 \times 10^{-10}, \quad (84)$$

where the errors associated with the individual classes of missing diagrams have been added linearly. If a_μ^{SUSY} is approximated by only the first line of (79), the error increases by the neglected contributions in the second line. An upper limit of these can be well approximated by [48, 49]

$$\delta a_\mu^{\text{SUSY}}(\text{2nd line}) = 0.3 \left(a_\mu^{(\chi\gamma H)} + a_\mu^{(\tilde{f}\gamma H)} \right) + 0.3 \times 10^{-10}. \quad (85)$$

It should be noted that the error estimate is deliberately conservative. The later numerical analysis, see e.g. table 2, shows that often already the known two-loop contributions are much smaller than 10^{-10} . In these cases, it is reasonable to assume that the theory error due to the unknown higher-order corrections is also much smaller than the estimate (84). In any case, the theory error of the SUSY contributions is smaller than both the current SM theory error and the experimental uncertainty.

3. Numerical behaviour of the SUSY contributions

The SUSY contributions to a_μ depend on the MSSM parameters in a complicated way. In this section we analyze the parameter dependence of the numerical results in detail. For each of the one- and two-loop contributions to a_μ we will describe which parameters are more and which are less influential and explain the dominant behaviour. We discuss the parameter choices for which each contribution can become particularly large and the numerical values that can be expected for various typical parameter choices. Finally, we provide the values of the SUSY contributions to a_μ for the benchmark ‘‘SPS’’ reference points [64].

3.1. One-loop contributions

The generic behaviour of the SUSY one-loop contributions to a_μ is well described by (80). The suppression by $1/M_{\text{SUSY}}^2$, the enhancement $\propto \tan\beta$ and the dependence on the sign of μ has been explained in section 2.1 using mass insertion diagrams. This generic $\tan\beta \text{sign}(\mu)$ behaviour is illustrated by figure 7, which shows $a_\mu^{\text{SUSY,1L}}$ for various values

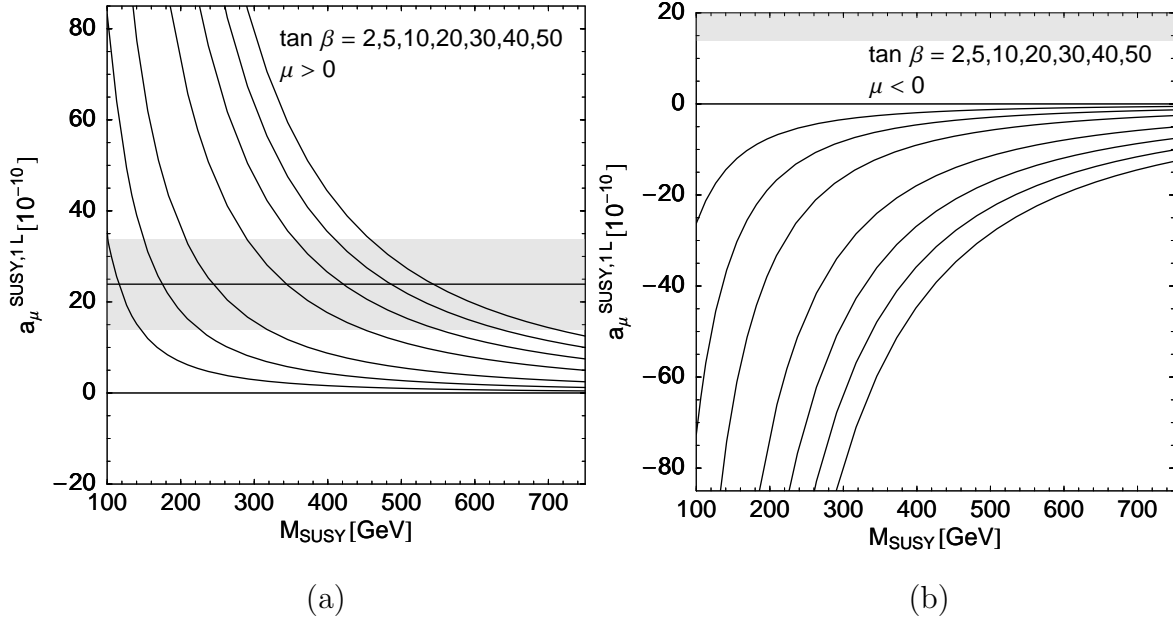


Figure 7. $a_\mu^{\text{SUSY,1L}}$ as a function of a common mass scale $M_{\text{SUSY}} = |\mu| = M_2 = m_{L,\tilde{\mu}} = m_{R,\tilde{\mu}}$ for various values of $\tan \beta$ and $\mu > 0$ (panel (a)), $\mu < 0$ (panel (b)). The smaller values of $\tan \beta$ correspond to smaller $|a_\mu^{\text{SUSY,1L}}|$. The preferred 1σ region (5) is indicated in grey.

of $\tan \beta$ and both signs of μ . A common mass scale $|\mu| = M_2 = m_{L,\tilde{\mu}} = m_{R,\tilde{\mu}} \equiv M_{\text{SUSY}}$ has been chosen, except that M_1 is fixed by the GUT relation $M_1/M_2 = 5g_1^2/3g_2^2$ and $A_\mu = 0$. Only for small $\tan \beta$ there are visible deviations from this simple behaviour due to formally $1/\tan \beta$ -suppressed terms. The figure also demonstrates that $a_\mu^{\text{SUSY,1L}}$ can be well in agreement with the observed deviation (5), but the small uncertainty in (5) results in stringent constraints on SUSY parameters. In the following we consider the $\tan \beta \text{ sign}(\mu)$ dependence as understood and fix μ to be positive and $\tan \beta$ to be large.

3.1.1. Dependence on mass parameters In general, $a_\mu^{\text{SUSY,1L}}$ depends on $\tan \beta$ and six mass parameters $\mu, M_{1,2}, m_{L,\tilde{\mu}}, m_{R,\tilde{\mu}}, A_\mu$. In the following we will first concentrate on the behaviour of $a_\mu^{\text{SUSY,1L}}$ as a function of the four parameters

$$\mu, M_2, m_{L,\tilde{\mu}}, m_{R,\tilde{\mu}} \quad (86)$$

and fix M_1 by the GUT relation $M_1/M_2 = 5g_1^2/3g_2^2 \approx 1/2$ and set $A_\mu = 0$.

We visualize the behaviour of $a_\mu^{\text{SUSY,1L}}$ for $\tan \beta = 50$ in this four-dimensional parameter space with the help of figure 8. In this figure, M_2 is chosen to be the smallest of the four mass parameters, and $\mu, m_{L,\tilde{\mu}}, m_{R,\tilde{\mu}}$ are independently varied in the range $M_2 \dots 5M_2$. The left and right panels correspond to the choices $m_{L,\tilde{\mu}} = M_2$ (panel (a)) and $m_{L,\tilde{\mu}} = 5M_2$ (panel (b)). The different colours correspond to the values $\mu = M_2$ (dark blue) and $\mu = 5M_2$ (light yellow). In all regions, the right-handed smuon mass is varied between $m_{R,\tilde{\mu}} = (1 \dots 5)M_2$. Keeping these parameter ratios fixed, M_2 is varied, and the resulting $a_\mu^{\text{SUSY,1L}}$ is plotted as a function of the mass M_{LOSP} of the lightest

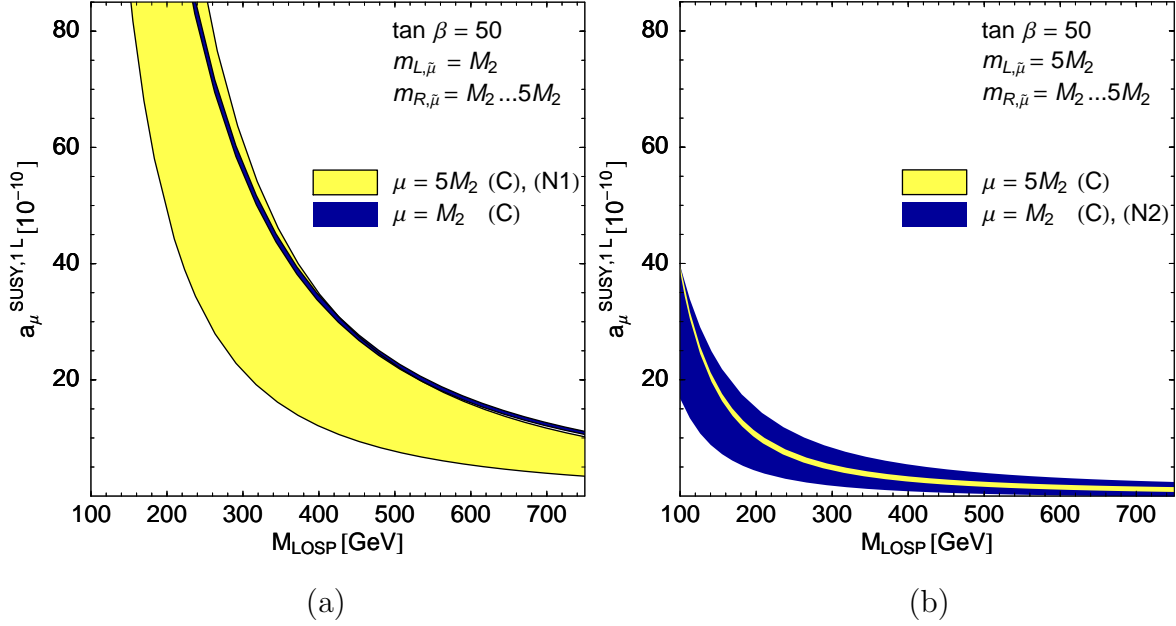


Figure 8. $a_\mu^{\text{SUSY,1L}}$ as a function of the mass of the lightest observable supersymmetric particle M_{LOSP} , for $\tan\beta = 50$ and the mass parameters varied in the range $M_2 \dots 5M_2$. The blue (yellow) regions correspond to $\mu = M_2$ ($\mu = 5M_2$) and $m_{R,\tilde{\mu}} = (1 \dots 5)M$. In panel (a), the left-handed smuon mass is small, $m_{L,\tilde{\mu}} = M_2$, in panel (b) $m_{L,\tilde{\mu}} = 5M_2$. For each case it is indicated which of the mass-insertion diagrams (C), (N1), (N2) are dominant.

observable SUSY particle [65], defined here as $\min(m_{\tilde{\mu}_1}, m_{\chi_1^\pm}, m_{\chi_2^0})$.

The two panels show that the μ -dependence is quite different for small and for large $m_{L,\tilde{\mu}}$. This intricate interplay between the parameters has been first studied in [44], where it has been shown that the mass-insertion diagrams of figure 2 provide an intuitive understanding of the parameter-dependence. In general, the chargino-diagram (C) dominates due to its large numerical prefactor in (58). In special parameter regions, the diagrams (N1) with bino-exchange and (N2) with $\tilde{\mu}_R$ -exchange can become important.

- *Panel (a), dark blue:* In the simple case $\mu = m_{L,\tilde{\mu}} = M_2$, the chargino diagram (C) dominates. There is hardly any suppression for heavy $m_{R,\tilde{\mu}}$, which enters only via the smaller neutralino diagrams. Therefore the corresponding dark blue region in panel (a) is very narrow.
- *Panel (a), light yellow:* If μ is increased, the chargino and most neutralino diagrams are suppressed. For large μ the largest contribution can come from the bino-diagram (N1), which is linear in μ . However, (N1) is only large if both left- and right-handed smuons are light. The large spread of the yellow region in panel (a) corresponds mainly to this $m_{R,\tilde{\mu}}$ -dependence of (N1). The upper border corresponds to small $m_{R,\tilde{\mu}}$ (i.e. to $\mu = 5M_2$, $m_{L,\tilde{\mu}} = m_{R,\tilde{\mu}} = M_2$) and leads to values of $a_\mu^{\text{SUSY,1L}}$ that are even larger than the ones in the blue region. This shows that the largest $a_\mu^{\text{SUSY,1L}}$ for a given value of M_{LOSP} is obtained for $\mu \gg m_{L,R,\tilde{\mu}}, M_2$ via diagram (N1). The values at the lower border are suppressed by the large $m_{R,\tilde{\mu}} = 5M_2$ and are roughly

by a factor 3 smaller.

- *Panel (b), light yellow:* The situation is reversed in panel (b) for large $m_{L,\tilde{\mu}}$. In this case large μ does not lead to an enhancement of diagram (N1) or any other diagram, since then all diagrams are suppressed either by the large μ or the large $m_{L,\tilde{\mu}}$. Consequently the result for $\mu = m_{L,\tilde{\mu}} = 5M_2$ is dominated by diagram (C) and is almost independent of $m_{R,\tilde{\mu}}$. Hence the yellow region in panel (b) is narrow.
- *Panel (b), dark blue:* For large $m_{L,\tilde{\mu}}$ but small μ , however, diagram (N2) with $\tilde{\mu}_R$ -exchange becomes important. It is the unique diagram that is not suppressed by the large $m_{L,\tilde{\mu}}$, but it has the opposite sign and a smaller numerical prefactor than diagram (C). The lower border of the blue region in panel (b) corresponds to the case of small $m_{R,\tilde{\mu}}$, i.e. to $m_{R,\tilde{\mu}} = \mu = m_{L,\tilde{\mu}}/5$, where the contributions of (C) and (N2) almost cancel. For larger ratios than displayed in the plot, $m_{L,\tilde{\mu}}/m_{R,\tilde{\mu}} > 5$, $a_\mu^{\text{SUSY,1L}}$ can even change sign. The upper border of the same region corresponds to the case of large $m_{R,\tilde{\mu}}$, where (C) dominates and (N2) is suppressed.

Figure 9 shows how the results are modified for different choices of M_2 and $\tan\beta$. Generally, larger values of M_2 lead to a suppression of the results without dramatic change of the qualitative behaviour, and smaller values of $\tan\beta$ lead to a suppression of the results due to the almost linear $\tan\beta$ -dependence. Figure 9 (a) shows the same as figure 8 (a) except that M_2 has been replaced by $5M_2$, i.e. M_2 is the largest of the four mass parameters and the other three are varied between $M_2/5 \dots M_2$. We find that the qualitative features are essentially unchanged. The larger value of M_2 leads to a suppression by a factor of roughly 3, and the largest contributions are now obtained for small $\mu = M_2/5$, corresponding to the dark blue region. Panel (b) shows the same again but for $\tan\beta = 5$ (and small M_2). Here the results are reduced by almost a factor 10 compared to the case with $\tan\beta = 50$, as expected.

The two mass parameters we have not explicitly discussed yet are A_μ and M_1 . M_1 has generally less influence than M_2 since the M_1 -independent chargino diagrams dominate in most of the parameter space. However, as exemplified by the discussion of figure 8 (a) there are situations where the bino-exchange diagram (N1) becomes important. If M_1 is not tied to M_2 by the GUT relation, it is possible to choose $M_2, \mu \gg M_1$. In this case one can obtain large contributions to $a_\mu^{\text{SUSY,1L}}$ from diagram (N1) even if both charginos are very heavy [47].

The dependence of $a_\mu^{\text{SUSY,1L}}$ on A_μ arises only via the smuon mixing matrix, where A_μ is accompanied by the term $\mu \tan\beta$, which is typically much larger. Therefore, A_μ is quite insignificant for the SUSY contributions to a_μ . The small influence of A_μ was verified in [65] by means of a scan of the SUSY parameter space, where $|A_\mu|$ was varied up to 100 TeV.

3.1.2. CP violation and flavour violation So far, we have neglected the possibilities of complex phases and generation mixing in the SUSY parameters. The influence of complex phases has been studied in [47,66,67]. Clearly, the phase of the μ -parameter has

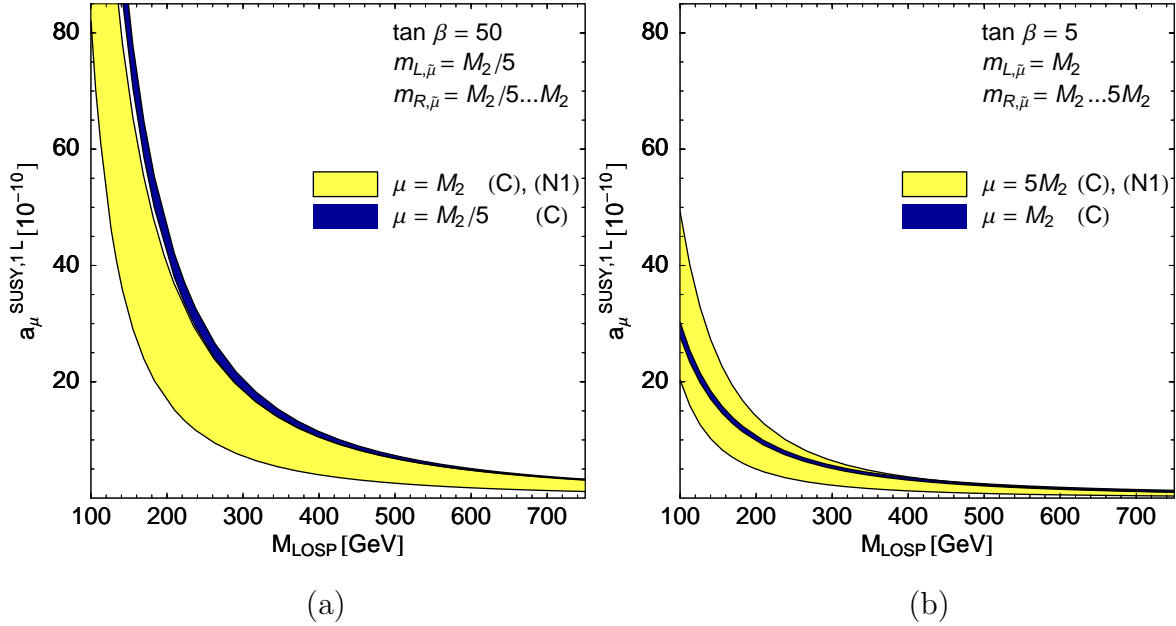


Figure 9. $a_\mu^{\text{SUSY,1L}}$ as a function of the mass of the lightest observable supersymmetric particle M_{LOSP} , for the same parameters as in figure 8 (a), except $M_2 \rightarrow 5M_2$ (left panel), $\tan \beta = 5$ (right panel).

the most significant impact, corresponding to the $\text{sign}(\mu)$ -dependence in the real case. At the same time, this phase is strongly restricted by negative results for electric dipole moment (EDM) measurements. Nevertheless, non-negligible effects of the complex phases can be obtained [66, 67] even if only small phases that do not violate the EDM-bounds are considered. On the other hand, CP invariance is not a critical symmetry for the magnetic moment, in contrast to e.g. chiral invariance. Therefore, CP-violating phases do not lead to new enhancement factors, and the largest SUSY contributions are naturally obtained for real parameters [47].

The situation is different for generation mixing in the slepton sector. If the smuons can mix with staus, it is possible to obtain contributions where the chirality is flipped at a stau-line instead of a smuon-line and thus contributes a factor m_τ instead of m_μ [44]. An example is provided by diagram (N1), where the $\tilde{\mu}_L\text{--}\tilde{\mu}_R$ insertion is replaced by a $\tilde{\tau}_L\text{--}\tilde{\tau}_R$ insertion. Due to the large enhancement factor m_τ/m_μ , even a small smuon–stau mixing can lead to sizable corrections to $a_\mu^{\text{SUSY,1L}}$ [44].

3.2. Two-loop contributions

3.2.1. Chargino/neutralino-loop contributions The two-loop contributions from closed chargino/neutralino loops have the same linear $\tan \beta$ -dependence and $1/M_{\text{SUSY}}^2$ -suppression as the one-loop contributions, see (81). The detailed parameter-dependence, however, shows interesting differences, as shown in [49].

In contrast to the one-loop contributions, the two-loop chargino/neutralino diagrams are independent of the smuon mass parameters. They only depend on μ ,

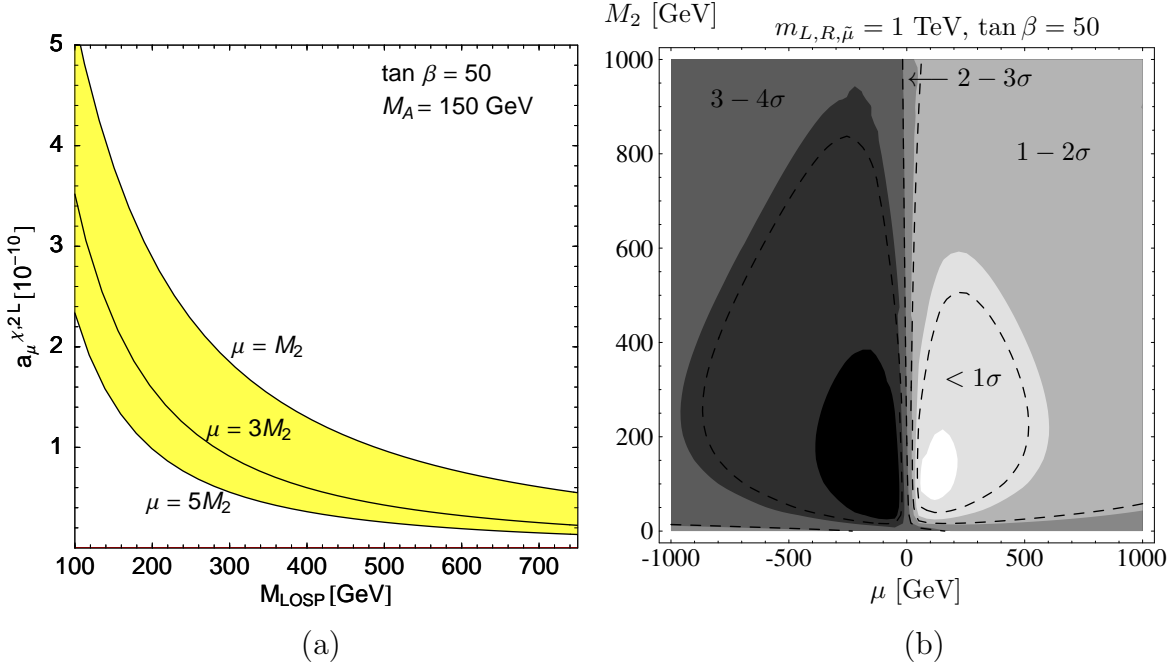


Figure 10. Panel (a): $a_\mu^{(x^{VH}), (x^{VV})}$ as a function of the mass of the lightest observable supersymmetric particle $M_{\text{LOSP}} = \min(m_{\chi_1^\pm}, m_{\chi_2^0})$, for $\tan \beta = 50$ and $M_A = 150$ GeV and for three different ratios $\mu/M_2 = 1, 3, 5$ (from top to bottom). Panel (b): Contours of $a_\mu^{\text{SUSY, 1L}} + a_\mu^{(x^{VH}), (x^{VV})}$ (solid border) and $a_\mu^{\text{SUSY, 1L}}$ alone (dashed line) in the $(\mu - M_2)$ -plane for $M_A = 200$ GeV, $m_{L,R,\tilde{\mu}} = 1000$ GeV and $\tan \beta = 50$. The contours are at $(24.5, 15.5, 6.5, -2.5, -11.5, -20.5) \times 10^{-10}$. Likewise, the colours of the fully drawn areas correspond to the following values: white: $> 24.5 \times 10^{-10}$, lightest grey: $(15.5 \dots 24.5) \times 10^{-10}, \dots$, black: $< -20.5 \times 10^{-10}$. The plot has been taken from [49], and the contours and regions correspond to $\Delta a_\mu(\text{exp} - \text{SM})$ as taken in that reference.

$M_{1,2}$, and the Higgs boson mass M_A . Moreover, the dependence on these parameters is quite straightforward, while the μ -dependence at the one-loop level is very complicated due to the different behaviour of diagrams (C), (N1) in figure 2, for example.

Figure 10 (a) shows the result of the two-loop chargino/neutralino contributions $a_\mu^{(x^{VH}), (x^{VV})}$ for three different ratios $\mu/M_2 = 1, 3, 5$ as a function of M_{LOSP} , defined here as $\min(m_{\chi_1^\pm}, m_{\chi_2^0})$. The other parameters are chosen as $\tan \beta = 50$ and $M_A = 150$ GeV, and the bino mass parameter M_1 is determined by M_2 via the GUT relation. For $M_{\text{LOSP}} > 100$ GeV, contributions of up to 5×10^{-10} can be obtained. This is a lot smaller than the largest possible one-loop contributions, but it can be a significant correction if the one-loop contributions are suppressed by heavy smuons and sneutrinos.

This can be seen immediately by comparing the two-loop contributions in figure 10 (a) with the one-loop contributions in the blue region in figure 8 (b), where $m_{L,\tilde{\mu}} = 5M_2 = 5\mu$. In this case the two-loop correction can amount to more than 20% of the one-loop result.

The result for a given M_{LOSP} is largest if μ and M_2 are equal. There is no enhancement for larger μ similar to the one-loop diagram (N1). Instead, increasing μ to $\mu = 5M_2$ leads to a suppression of the result by a factor $2 \dots 3$; for even larger

ratios than the ones displayed in the figure, the result becomes even smaller.

For larger values of M_A , the result is suppressed as well. We have checked that the results in figure 10 (a) would be smaller by a factor 1.5 (for large M_{LOSP}) to 2.5 (for small M_{LOSP}) for $M_A = 300$ GeV instead of 150 GeV. This is in agreement with the analysis of the M_A -dependence in [49] for a wider selection of values for μ and M_2 .

Figure 10 (a) does not contain the case $\mu < M_2$. It is straightforward to show from the exact expression (63) that the dominant contribution $a_\mu^{(\chi\gamma H)}$ is symmetric under the exchange $\mu \leftrightarrow M_2$. Therefore the behaviour for $\mu < M_2$ is very similar to the one for $\mu > M_2$ and does not need to be analyzed separately.

The importance of the two-loop corrections is also visible in figure 10 (b), which has been taken from [49]. Here the one-loop contributions and the sum of one- and two-loop corrections are shown in a contour plot in the $(\mu-M_2)$ -plane. The smuon mass parameters are heavy, $m_{L,R,\tilde{\mu}} = 1000$ GeV, and $\tan\beta = 50$, $M_A = 200$ GeV. The white and lightest grey regions correspond to the 1σ -region around the experimentally preferred value (the value $24.5(9.0) \times 10^{-10}$ used for the plot is very similar to the one quoted in (5)). For the chosen parameters, this region extends up to $\mu, M_2 \leq 600$ GeV. However, it is clearly visible that if the two-loop contributions were neglected, the contours would shift considerably, and the 1σ region would extend only up to $\mu, M_2 \leq 500$ GeV.

3.2.2. Sfermion-loop contributions The two-loop contributions from sfermion-loop diagrams can be even larger than the ones from chargino/neutralino-loop diagrams. As discussed in [48, 59, 60], however, and as the discussion in section 2.1 and formulas (82), (83) show, these large contributions arise only in special corners of parameter space. The stop-loop diagrams become large if the stop mixing is large, one stop is light, μ is very large and M_A is small. Similarly, sbottom-loop diagrams become large for large sbottom mixing and if A_b/M_A is very large.

Such parameter regions are quite restricted for several reasons. Primarily, small stop or sbottom masses in conjunction with large $\tan\beta$ can have dramatic effects on the SUSY predictions for the lightest Higgs boson mass and b -decays and are therefore constrained by experimental limits on these observables. Furthermore, large μ is restricted by the requirement that the sbottom mass eigenvalues are positive, and by naturalness arguments due to its appearance in the Higgs potential.

Figure 11 (a) shows the results of the two-loop contributions from sfermion-loop diagrams as a function of the lightest sfermion mass in two particular parameter scenarios. The parameters have been chosen such that they are in agreement with experimental bounds and that the results are sizable. The Higgs boson mass $M_A = 300$ GeV, $\tan\beta = 50$, the sfermion mass parameters $m_{L,\tilde{t}}, m_{R,\tilde{t}}, m_{R,\tilde{b}}, m_{L,\tilde{\tau}}, m_{R,\tilde{\tau}}$ have been chosen equal to a common scale M_{SUSY} . The trilinear parameter $A_t = -2M_{\text{SUSY}}$, which leads to maximal stop mixing and values of M_h , evaluated using *FeynHiggs* [68–71] including higher-order corrections, which are in agreement with current bounds.

The light yellow region of figure 11 (a) corresponds to $\mu = -A_t = 2M_{\text{SUSY}}$ and thus

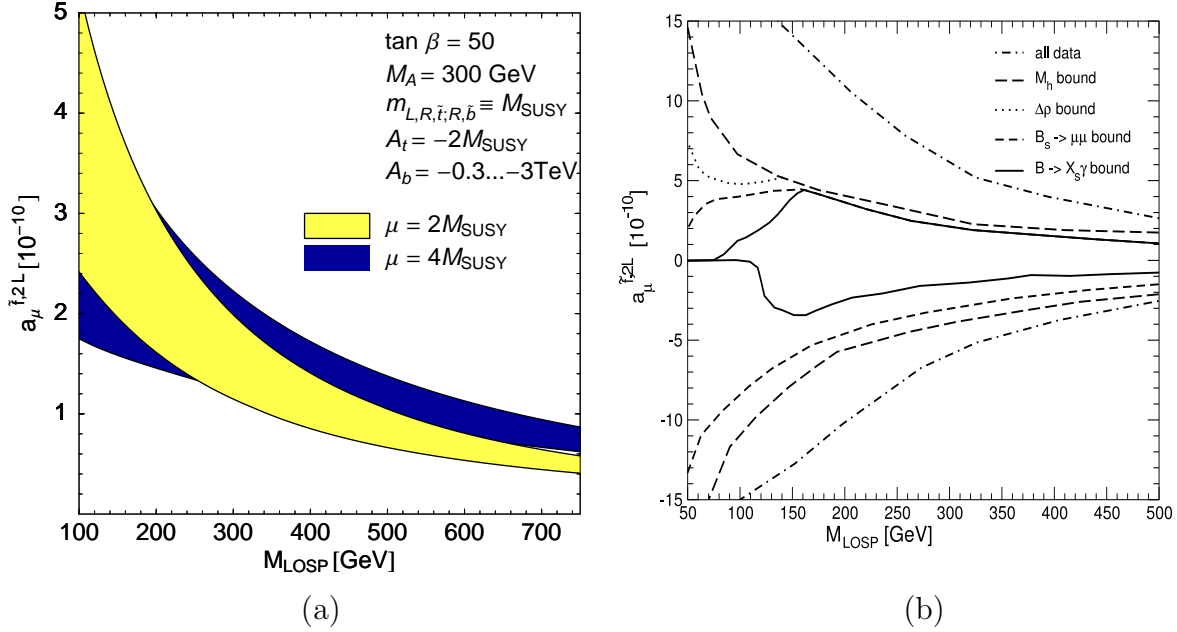


Figure 11. Panel (a): $a_\mu^{\tilde{f},2L}$ as a function of the mass of the lightest observable supersymmetric particle $M_{\text{LOSP}} = \min(m_{\tilde{t}_1}, m_{\tilde{b}_1})$, for the parameter values given in the plot. The light yellow (dark blue) region corresponds to $\mu = -A_t = 2M_{\text{SUSY}}$ ($\mu = -2A_t = 4M_{\text{SUSY}}$), where M_{SUSY} is the common sfermion mass parameter, and $A_b = A_\tau = 300 \dots 3000$ GeV. Panel (b): Maximum values of $a_\mu^{\tilde{f},2L}$ obtained in a parameter scan in the region (87) if the experimental constraints described in the text are incrementally applied. The plot has been taken from [48].

to a situation where the lightest stop and sbottom masses are approximately equal. In the dark blue region, $\mu = -2A_t = 4M_{\text{SUSY}}$, and thus the lightest sbottom is significantly lighter than the lightest stop. In both regions, $A_b = A_\tau = -300 \dots -3000$ GeV. The signs of the parameters are such that the sbottom and stop contributions add up constructively. The lower borders of the yellow and blue bands correspond to small $|A_b|$ and thus mainly to the pure stop-loop contributions. The width of the bands is essentially due to the sbottom-loop contributions, which are approximately linear in A_b .

The larger value of μ in the blue region has two effects. On the one hand, the lightest sbottom is lighter than the lightest stop, and thus the sbottom-loop contributions have more relative importance. Hence the blue band is wider than the yellow band. On the other hand, since the stop-loop contributions increase linearly with μ , they are enhanced as well in spite of the heavier stops, and hence the blue band lies at higher values of $a_\mu^{\tilde{f},2L}$.

The upper borders of the two bands almost exhaust the limits found in [48] for the largest possible values of $a_\mu^{\tilde{f},2L}$. Figure 11 (a), taken from [48], shows these largest possible values depending on which experimental constraints are taken into account. The allowed parameter range is

$$\tan\beta = 50, \quad M_{\text{SUSY}} \leq 1 \text{ TeV}, \quad |\mu|, |A_{t,b}| \leq 3 \text{ TeV}, \quad 150 \text{ GeV} \leq M_A \leq 1 \text{ TeV} \quad (87)$$

with common sfermion mass parameters $m_{L,\tilde{t}} = m_{R,\tilde{t}} = m_{R,\tilde{b}} = m_{L,\tilde{\tau}} = m_{R,\tilde{\tau}} = M_{\text{SUSY}}$

and $A_\tau = A_b$. The experimental constraints are $M_h > 106.4$ GeV, $\Delta\rho^{\text{SUSY}} < 4 \times 10^{-3}$, $\text{BR}(B_s \rightarrow \mu^+\mu^-) < 1.2 \times 10^{-6}$, $|\text{BR}(B \rightarrow X_s\gamma) - 3.34 \times 10^{-4}| < 1.5 \times 10^{-4}$, corresponding to conservative bounds taking into account experimental and theoretical uncertainties (see [48] and references therein).

If all experimental constraints are ignored, $a_\mu^{\tilde{f},2\text{L}} > 15 \times 10^{-10}$ is possible, in agreement with the results of [59,60]. Taking into account the Higgs boson mass limit reduces the maximum contributions drastically, and if all constraints are taken into account $a_\mu^{\tilde{f},2\text{L}}$ turns out to be smaller than 5×10^{-10} in the parameter region (87).[§]

Significantly larger values of these contributions can be obtained if the sfermion mass parameters are non-universal. In particular, if the ratio of $m_{R,\tilde{b}}$ and $m_{R,\tilde{t}}$ is either very large or very small, values of $a_\mu^{\tilde{f},2\text{L}} > 15 \times 10^{-10}$ can be in agreement with all experimental constraints [48]. We will come back to this possibility in section 4.6, where general scans of the MSSM parameter space are described.

3.3. Results for SPS benchmark points

After having discussed the general parameter dependence of the individual SUSY contributions to a_μ , we present here the results obtained in the Snowmass Points and Slopes (SPS) benchmark points [64]. These results provide an overview and reference of the SUSY contributions that can be expected in various well-motivated and often considered parameter scenarios. Furthermore, we use these results to assess the relative importance of the individual one- and two-loop contributions.

Table 2 shows the results of the known contributions to a_μ^{SUSY} , split up according to (79). The QED-improved one-loop and the two-loop contributions with photon exchange in the first line of (79) are listed explicitly. The remaining contributions are combined into the ones from diagrams with charginos, neutralinos or sfermions and the purely SM-like ones.

The SPS points 1a, 1b, 3, 6 correspond to various minimal supergravity (mSUGRA)-scenarios with $\tan\beta$ between 10 and 30 and SUSY masses in the range 100...1000 GeV. They lead to predictions of a_μ very close to the observed value (5). The same is true for points 7, 8, which correspond to gauge-mediated SUSY breaking. The point SPS 2 does not fit so well to (5) because it corresponds to the focus-point region in which sfermions are very heavy. SPS 4, 5 involve very large/small $\tan\beta$, respectively, and therefore yield too high/low values for a_μ^{SUSY} , and SPS 9, which corresponds to anomaly-mediated SUSY breaking, involves negative ($\mu M_{1,2}$) and thus leads to negative a_μ^{SUSY} .

The two-loop corrections are very small in all cases. In general, the chargino- or sfermion-loop contributions with photon exchange can be the largest two-loop contributions, but in all SPS points they are suppressed by moderate values of $\tan\beta$

[§] For very low sfermion masses the parameter scenarios used in figure 11 (a) violate the experimental bounds, which is why the results displayed in figure 11 (a) are larger than the limits found in figure 11 (b) at $M_{\text{LOSP}} \approx 100$ GeV.

Table 2. Results of the SUSY contributions to a_μ in units of 10^{-10} for the SPS benchmark parameter points. The one-loop contributions include the two-loop QED-logarithms (78). The SUSY two-loop corrections to SM one-loop diagrams have been split up as $a_\mu^{\text{SUSY,2L(a)}} = a_\mu^{(\chi\gamma H)} + a_\mu^{(\tilde{f}\gamma H)} + a_\mu^{\text{SUSY},\chi+\tilde{f},\text{rest}} + a_\mu^{\text{SUSY,ferm+bos,2L}}$ into the photon-loop contributions, the remaining chargino/neutralino and sfermion contributions, and the bosonic and fermionic contributions.

SPS Point	$a_\mu^{\text{SUSY,1L(improved)}}$	$a_\mu^{(\chi\gamma H)}$	$a_\mu^{(\tilde{f}\gamma H)}$	$a_\mu^{\text{SUSY},\chi+\tilde{f},\text{rest}}$	$a_\mu^{\text{SUSY,ferm+bos,2L}}$
SPS 1a	29.29	0.168	0.029	0.056	0.267
SPS 1b	31.84	0.273	0.044	0.106	0.222
SPS 2	1.65	0.032	-0.002	0.027	0.068
SPS 3	13.55	0.078	0.009	0.029	0.187
SPS 4	49.04	0.786	0.085	0.288	0.349
SPS 5	8.59	0.029	0.135	-0.046	0.153
SPS 6	16.87	0.125	0.015	0.044	0.230
SPS 7	23.71	0.236	0	0.089	0.282
SPS 8	17.33	0.163	-0.001	0.062	0.211
SPS 9	-8.98	-0.046	-0.002	-0.018	0.115

and/or rather high values of M_A . Particularly the sfermion-loop contributions are suppressed in addition by the heavy stops and sbottoms in all points except SPS 5. The results show, however, that the photon-exchange contributions are larger than $a_\mu^{\text{SUSY},\chi+\tilde{f},\text{rest}}$ by a factor ≈ 3 , in agreement with the discussion in section 2.3.1 and the error estimate (85). Likewise, the two-loop corrections from SM-like diagrams with fermionic or bosonic loops are in the expected range $\approx (0.1 \dots 0.3) \times 10^{-10}$.

4. Impact on SUSY phenomenology

In this section we assume that the MSSM is the correct description of physics at the weak scale and above and interpret the muon $g-2$ measurement within this framework. We discuss the impact of the result for a_μ on the SUSY parameter space and its relation to other relevant observables.

The deviation $\Delta a_\mu(\text{exp} - \text{SM})$ is positive and larger than the pure SM weak contribution, see (5), (9), (10). We have seen before that the MSSM can easily accommodate this deviation, preferably for a rather small SUSY mass scale and/or large $\tan\beta$ and a positive μ -parameter. In the following, we first focus on the general MSSM and show that specific, quantitative upper and lower bounds on SUSY masses can be derived from a_μ . Then we compare a_μ to b -decays, the Higgs boson mass and electroweak observables, and neutralino dark matter. Several of these observables exhibit correlations with a_μ , while others lead to complementary information on SUSY parameters.

Parameter bounds as well as correlations between observables become much more

severe in more constrained models than the MSSM. We discuss here the cases of minimal supergravity, gauge-mediated SUSY breaking and anomaly-mediated SUSY breaking. We conclude the section with a full parameter scan in the general MSSM that summarizes the current status of a_μ in SUSY.

4.1. Constraints from a_μ on the general MSSM

Already before the Brookhaven $g - 2$ experiment, the muon magnetic moment was an important observable in SUSY phenomenology. Since the SM theory prediction agreed with the older CERN measurement of a_μ [19], it was possible to derive lower bounds on SUSY masses [33–43]. Even after many of these bounds were superseded by LEP bounds, taking into account a_μ remained complementary in corners of parameter space where light SUSY particles could escape LEP detection [72].

In 2001, the publication of the Brookhaven result [3] caused a lot of excitement since it showed a deviation of $43(16) \times 10^{-10}$ (2.6σ) from the SM theory prediction at the time (which involved a sign error in the light-by-light contributions). Many authors interpreted this result as a possible signal for supersymmetry, and a_μ was studied in general SUSY models [20, 47, 65, 73–81], with emphasis on correlations and implications for particular other observables [82–88], and special scenarios or extended models were considered [89–96]. A general conclusion was that significant constraints, in particular upper mass limits could be derived even in the general MSSM.

The current deviation (5) between the corrected SM result and the final experimental value is $23.9(9.9) \times 10^{-10}$. This is smaller but statistically almost as significant as the one in 2001, and it still allows to stringently constrain the MSSM parameter space. Without assuming any specific scenario of SUSY breaking it is possible to derive both *lower* and *upper* bounds on the masses of SUSY particles. It is particularly encouraging that not only one but several SUSY masses can be bounded from above.

Figure 12 from [97] shows the maximum values of the four lightest SUSY particle masses, depending on the value of a_μ^{SUSY} and $\tan\beta$. These values are obtained from a scan of the parameters M_2 , $m_{L,\tilde{\mu}}$, $m_{R,\tilde{\mu}}$, μ up to 2 TeV, assuming the GUT relation for M_1 . The bounds are independent of the identity of the SUSY particles but they mainly restrict the chargino/neutralino and smuon/sneutrino masses as these are most relevant for a_μ^{SUSY} . The figure shows meaningful bounds even for the fourth lightest SUSY particle. For example, for $\tan\beta = 10$, requiring that $a_\mu^{\text{SUSY}} > 14 \times 10^{-10}$ ($a_\mu^{\text{SUSY}} > 4.1 \times 10^{-10}$), corresponding to a 1σ (2σ) band in (5), implies that four SUSY particles are lighter than about 500 GeV (1 TeV) and two of them are even lighter than 350 GeV (600 GeV). The upper mass limits are tighter for smaller values of $\tan\beta$, but all values of $\tan\beta$ allow for contributions a_μ^{SUSY} larger than 20×10^{-10} , so a_μ alone does not place a lower bound on $\tan\beta$ [47, 97].

The upper mass limits are very promising for the search for SUSY particles at the LHC and ILC. At a linear e^+e^- collider, SUSY particles can be pair-produced if they are lighter than half of the center-of-mass energy. At the LHC, weakly interacting particles

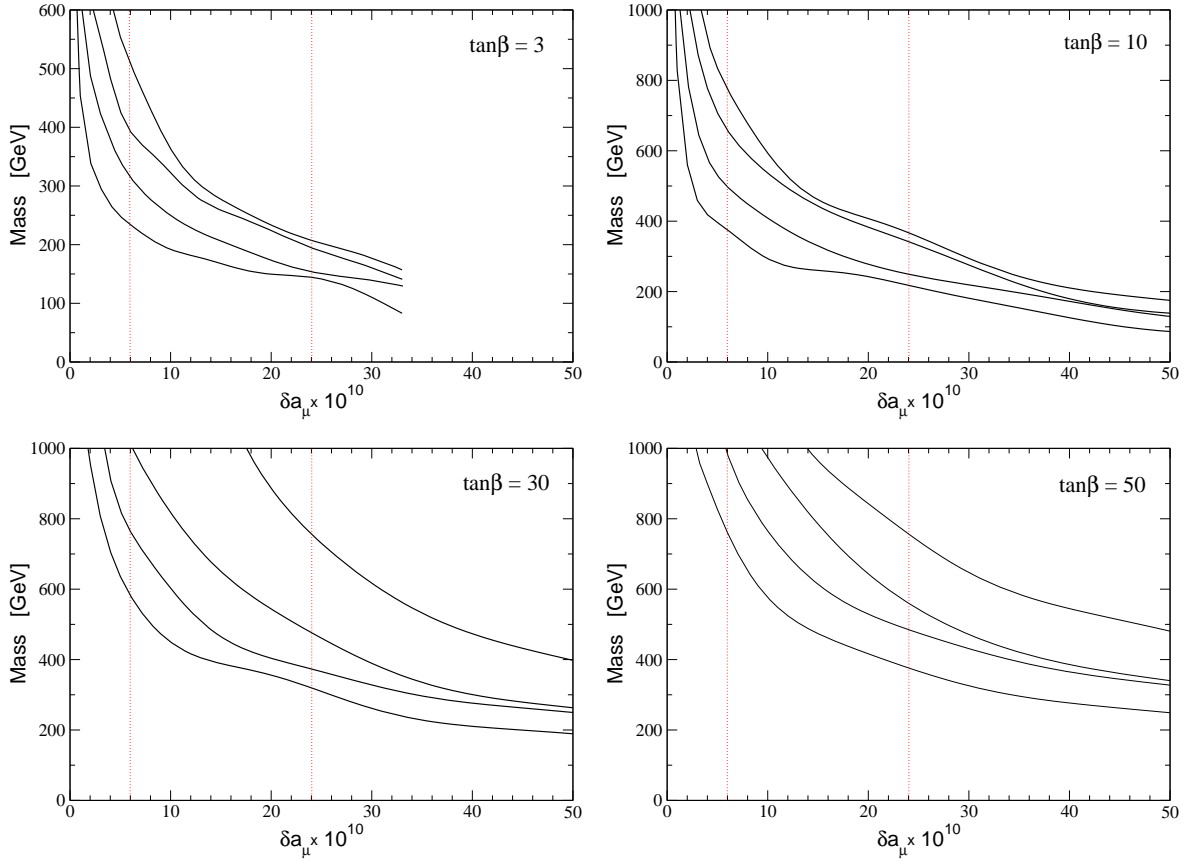


Figure 12. Upper bounds on the masses of the four lightest SUSY particles as a function of $\delta a_\mu \equiv a_\mu^{\text{SUSY}}$ for $\tan\beta = 3, 10, 30, 50$. The figure has been taken from [97], and the dotted vertical lines at $a_\mu^{\text{SUSY}} = 6, 24 \times 10^{-10}$ correspond to the -1σ lines according to two different SM theory evaluations (using or not using τ -decay data) available at the time of publication of [97]. Incidentally, they are close to the currently preferred value 23.9×10^{-10} and the lower 2σ contour 4.1×10^{-10} .

like charginos, neutralinos and smuons can be best studied in cascade decays of squarks, provided they are lighter than the squarks. In view of figure 12, combined with lower squark mass limits from Tevatron, these criteria might be satisfied for a number of SUSY particles.

One might argue that it is too aggressive to require that a_μ^{SUSY} is within the 1σ or 2σ band of (5), especially given the difficulty in assessing the theoretical errors of the SM hadronic contributions. Clearly, if e.g. a 3σ band is admitted, zero SUSY contributions are allowed, and the upper limits on SUSY masses disappear. However, interestingly even in a “super-conservative” approach significant parameter constraints can be derived [98]. The only requirement made in [98] was that a_μ^{SUSY} falls into the interval

$$-36.8 \times 10^{-10} < a_\mu^{\text{SUSY}} < 89.9 \times 10^{-10} \quad [98], \quad (88)$$

which was supposed to be a region that nobody could seriously argue with. At the

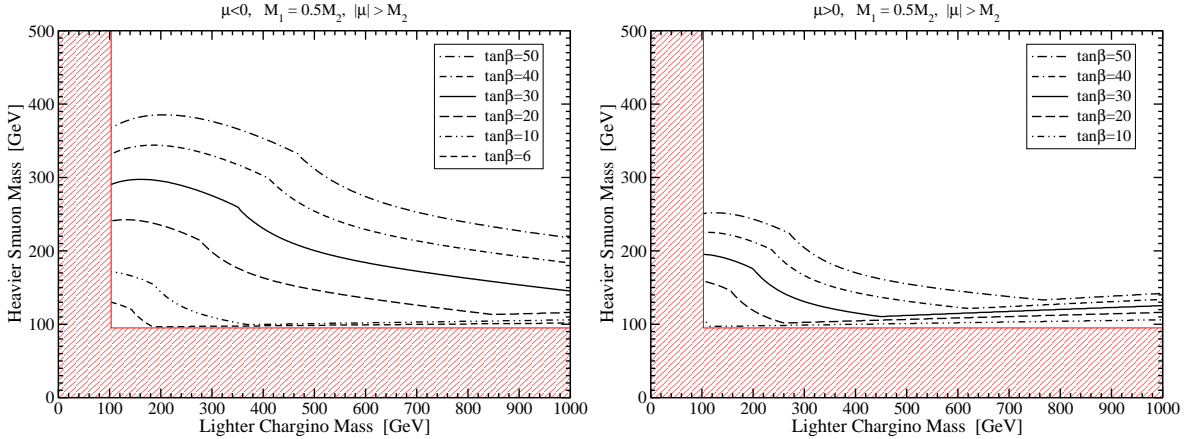


Figure 13. Lower mass bounds derived from the requirement that a_μ^{SUSY} lies in the super-conservative interval (88). For each $\tan\beta$ and $\text{sign}(\mu)$, the region below the corresponding line is excluded. The region constrained by direct searches is shaded. The figure has been taken from [98].

time of publication, it corresponded to the 5σ allowed region, now it corresponds roughly to the 6σ region. The bounds derived in [98] from (88) can therefore be regarded as definite bounds, independent of any future theoretical or experimental developments. In addition to (88), only the following assumptions have been made: all SUSY parameters are real, $|\mu| > M_2$, $M_1 = M_2/2$, smuon masses are greater than 95 GeV, and $|A_\mu|/m_{\tilde{\mu}_2} < 3$ in order to avoid electric charge-violating minima.

Figure 13 shows an example of the (lower) mass bounds that can be derived in this super-conservative approach in the plane of the lighter chargino and heavier smuon mass. For each $\tan\beta$, the region below the corresponding line is excluded. The excluded regions are larger for $\mu < 0$, reflecting the fact that a_μ favours positive μ . The excluded regions grow with $\tan\beta$, but even for small $\tan\beta$, a_μ excludes regions of parameter space that are not excluded by any other experiment.

4.2. General correlations with other observables

Many observables can be related to a_μ in a meaningful way. Here we discuss four particularly interesting examples: rare b -decays, the neutralino dark matter density and detection rate, the Higgs boson mass, and electroweak precision observables. Since the signs of the parameters play an important role, we fix the convention $M_2 > 0$ for simplicity in this and the following subsections.

We do not discuss in detail the possibility of lepton flavour violation. As mentioned in section 3.1.2, $\tilde{\mu}-\tilde{\tau}$ mixing can lead to substantial effects in a_μ^{SUSY} , and conversely the measurement of a_μ implies bounds on lepton flavour-violating parameters. Furthermore, the diagrams contributing to a_μ and processes like $\tau \rightarrow \mu\gamma$ and $\mu \rightarrow e\gamma$ have a similar structure and are correlated. Corresponding detailed studies can be found in [91, 94, 95, 99].

4.2.1. B-decays The rare b -decays $b \rightarrow s\gamma$ and $B_s \rightarrow \mu^+\mu^-$ are similar to a_μ in two respects. They are loop-induced, and they involve a chirality flip in the b - s transition. Correspondingly, the SUSY contributions to both branching ratios are enhanced by $\tan\beta$, in the second case even $\propto \tan^6\beta$. In the case of $b \rightarrow s\gamma$ also $\text{sign}(\mu)$ plays a crucial role as it determines whether diagrams with H^\pm exchange (always positive) and diagrams with chargino or gluino exchange (the leading terms are $\propto \text{sign}(\mu A_t)$, $\text{sign}(\mu M_3)$, respectively) interfere constructively or destructively. The current experimental results for the two branching ratios are [100,101]

$$\text{BR}(b \rightarrow s\gamma) = (3.39_{-0.27}^{+0.30}) \times 10^{-4}, \quad (89)$$

$$\text{BR}(B_s \rightarrow \mu^+\mu^-) < 1.0 \times 10^{-7} \quad (95\% \text{ C.L.}). \quad (90)$$

Since both results are well in agreement with the SM theory predictions, the possible SUSY contributions are bounded from above. As long as minimal flavour violation is assumed, this implies for example that destructive interference between the H^\pm and χ^\pm contributions to $b \rightarrow s\gamma$, and thus the specific $\text{sign } \mu A_t < 0$ is favoured (see [102,103] for reviews and references and [104] for a recent thorough analysis of b -physics and SUSY).

The interplay between rare b -decays and a_μ is particularly strong in the framework of specific models such as minimal supergravity or gauge-mediated SUSY breaking. Such models relate squark and slepton masses and make specific predictions on the signs of A_t and M_3 and thus also the sign of μ favoured by $b \rightarrow s\gamma$. Therefore an interesting tension can arise between $b \rightarrow s\gamma$ and a_μ . Both observables favour a particular sign of μ , but this might or might not be the same, depending on the values of A_t and M_3 . And both depend on $\tan\beta$ and SUSY masses, but a_μ prefers rather large and $b \rightarrow s\gamma$ rather small SUSY contributions.

4.2.2. Neutralino dark matter density and detection rate If the lightest neutralino is stable it provides a promising candidate for cold dark matter. In this case, two observables are of particular interest: the relic density and the detection rate, governed by the neutralino-nucleon cross section (for reviews and references see [105,106]). The spin-independent contribution σ_{SI} to this cross section is yet another chirality-flipping quantity, and it is also enhanced by large $\tan\beta$. Moreover, for positive μ this cross section is typically larger than 10^{-10} pb, which should be accessible to future detectors, while negative μ would allow for cancellations that could strongly suppress σ_{SI} , such that neutralino dark matter detection would be out of reach. Hence, the preference of a_μ for positive μ and not too small $\tan\beta$ has significant impact on the prospect of dark matter detection [74,78,82,107–110]. Figure 14 from [108] shows the spin-independent neutralino-nucleon cross section versus the neutralino mass for a wide range of the MSSM parameters μ , M_2 , $\tan\beta$, M_A , $A_{b,t}$, m_0 , where m_0 is a common sfermion mass parameter. The circles denote points that satisfy the a_μ constraint. Imposing this constraint increases the minimum value of σ_{SI} from 10^{-16} pb to 10^{-10} pb, significantly improving the prospect for direct detection of galactic neutralinos.

Under the assumption that standard cosmology (involving a fixed cosmological

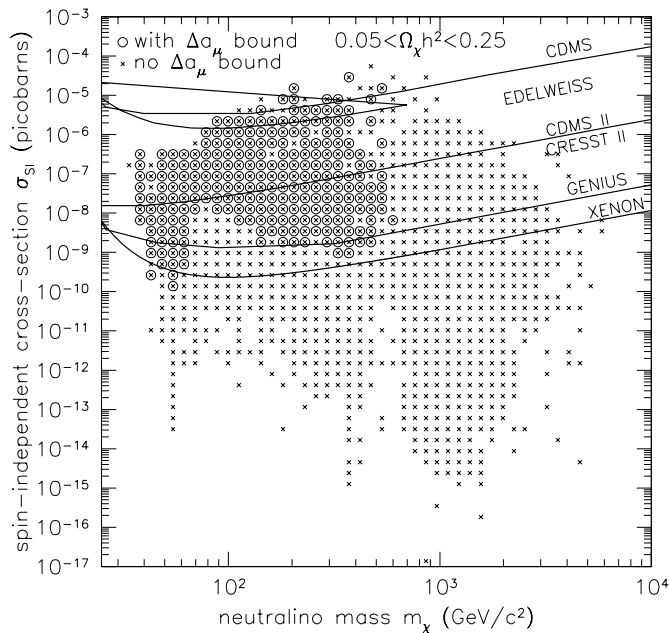


Figure 14. Neutralino–nucleon cross section versus neutralino mass, for a large range of MSSM parameters (see text), taken from [108]. Only those points are shown for which the neutralino relic density could account for all dark matter, but dropping this constraint does not affect the conclusions [108]. The circles denote points that satisfy the constraint $7 \times 10^{-10} < a_\mu^{\text{SUSY}} < 51 \times 10^{-10}$, corresponding to a 2σ range at the time of publication.

constant and a certain amount of cold dark matter) is valid and that neutralinos constitute the only component of cold dark matter, the neutralino relic density Ω_χ is fixed by astrophysical observations, in particular from WMAP [111]. Fixing Ω_χ effectively selects a one-dimensional hyper-surface from the MSSM parameter space. However, the dependence of Ω_χ on the MSSM parameters is rather uncorrelated with the one of a_μ . Hence, the measurement of a_μ and the increasingly precise determination of the cold dark matter density are complementary probes of the MSSM parameter space.

4.2.3. Lightest Higgs boson mass The lightest Higgs boson mass M_h is an important observable since it is tightly constrained in the MSSM. At tree level, M_h must be smaller than M_Z , but the current lower LEP-bound is $M_h > 114.4$ GeV (95% C.L.) [112]. Large quantum corrections can reconcile the MSSM prediction for M_h with the lower bound, but this leads to severe constraints on the MSSM parameter space. The main quantum corrections are enhanced by $m_t^4 \log(m_{\tilde{t}_1} m_{\tilde{t}_2} / m_{\tilde{t}}^2)$, and large $\tan\beta$ and large stop mixing can lead to further enhancements (see [27] for a review and references). Therefore, like

|| This bound applies only if the MSSM Higgs boson h is SM-like, which however is the case in the largest part of parameter space, in particular for $M_A \gtrsim 150$ GeV.

a_μ , the M_h -constraint favours larger $\tan\beta$, but unlike a_μ it also favours larger SUSY masses, at least in the stop sector.

Hence there can be a certain tension between the a_μ - and M_h -constraints, particularly in models that connect stop and smuon masses. This tension has become stronger recently owing to the latest determination $m_t = 171.4(2.1)$ GeV [113,114]. This value is lower than previous ones, and it increases the tendency of the M_h -constraint to favour rather large stop masses. In [115], the tension is illustrated for a class of SU(5) GUT models by plots of the largest possible a_μ^{SUSY} as a function of M_h . The higher the Higgs boson mass, the lower the possible values for a_μ^{SUSY} . However, the current bounds on a_μ and M_h can still be simultaneously satisfied in considerable parameter regions.

4.2.4. Electroweak precision observables Finally, we briefly comment on electroweak precision observables, particularly on M_W and the effective weak mixing angle $\sin^2\theta_{\text{eff}}$. The present experimental values are [114,116]

$$M_W^{\text{exp}} = 80.392(29) \text{ GeV}, \quad (91)$$

$$\sin^2\theta_{\text{eff}}^{\text{exp}} = 0.23153(16). \quad (92)$$

The SM predictions for these observables sensitively depend on the values of the SM input parameters, in particular on m_t and M_h . For the experimentally preferred values of the input parameters, the SM predictions agree with quite well M_W^{exp} and $\sin^2\theta_{\text{eff}}^{\text{exp}}$. It has been noted that the agreement with experiment can be even better in the MSSM (see e.g. [117] for an analysis that takes into account the most recent experimental data). The SUSY contributions to both observables are dominated by the quantity $\Delta\rho$, which is sensitive to the breaking of isospin invariance and thus e.g. to the mass splittings in the stop/sbottom sector. These SUSY contributions are enhanced for smaller stop/sbottom masses and also depend on the chargino and neutralino masses, but they are not particularly sensitive to $\tan\beta$. Therefore, a_μ as well as the electroweak precision observables have a tendency to favour not too heavy SUSY masses, and it is fruitful to combine analyses of both kinds of quantities [118–120].

4.3. MSUGRA

In the general MSSM, supersymmetry breaking is parametrized by a large set of free parameters. In specific scenarios of supersymmetry breaking these parameters find an explanation in terms of some underlying physical mechanism. Typically, then, the MSSM parameters can be related to a much smaller set of more fundamental quantities. Such supersymmetry breaking scenarios are very predictive, and parameter bounds implied by experimental constraints as well as correlations between observables are much more stringent than in the general MSSM.

The first scenario we discuss here is minimal supergravity (mSUGRA) and the very similar constrained MSSM (CMSSM) (see e.g. [121] and references therein). In this scenario supersymmetry breaking is assumed to take place in a hidden sector

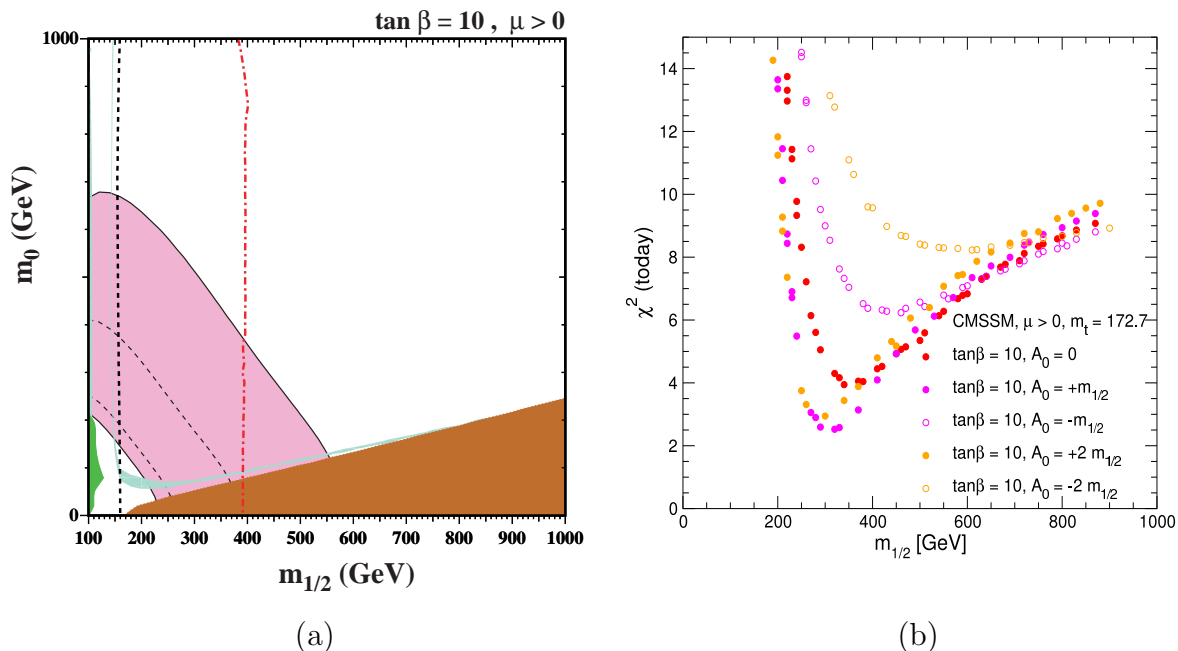


Figure 15. (a) The m_0 – $m_{1/2}$ plane of the CMSSM for $\mu > 0$, $\tan\beta = 10$, $A_0 = 0$, taken from [132]. The medium pink band and the thin black dashed lines show the 2σ and 1σ contours for a_μ . The near-vertical lines correspond to $M_h = 114$ GeV (red, dot-dashed), $m_{\chi_{1\pm}} = 104$ GeV (black, dashed); the medium green area is excluded by $b \rightarrow s\gamma$; and the light turquoise band satisfies the relic density constraint. In the dark red area the LSP is charged.

(b) Likelihood function χ^2_{tot} for the observables a_μ , $b \rightarrow s\gamma$, M_h , M_W , $\sin^2\theta_{\text{eff}}$ in the CMSSM for $\tan\beta = 10$ and various values of A_0 . m_0 is chosen to yield the central value of the relic density constraint. This figure has been taken from [120].

and to be transmitted to the observable sector via gravitational interactions. The Kähler potential of the underlying supergravity theory is assumed to be minimal, i.e. in particular to involve no generation-dependent couplings. Furthermore, at the GUT scale $M_{\text{GUT}} \approx 2 \times 10^{16}$ GeV the SM gauge interactions unify. The free parameters of this model are

$$m_0, m_{1/2}, A_0, \tan\beta, \text{sign}(\mu), \quad (93)$$

where m_0 , $m_{1/2}$ and A_0 are the universal values of all scalar mass, gaugino mass, and A parameters of the MSSM at the GUT scale. The low-energy values of the MSSM soft-breaking parameters are determined by renormalization-group running, and the value of $|\mu|$ is determined by the requirement that electroweak symmetry breaking leads to the correct value of M_Z . (The mSUGRA scenario also leads to a prediction of the gravitino mass, but in the present review we will not make use of this prediction.)

The phenomenology of mSUGRA has been studied extensively, in particular in view of the a_μ constraint (see [74, 77, 78, 81, 88, 122–124] for mSUGRA studies focussing on a_μ and [119, 120, 125–131] for recent general analyses of mSUGRA).

As an example, figure 15 (a) from [132] shows the mSUGRA m_0 – $m_{1/2}$ plane for

$A_0 = 0$, $\tan\beta = 10$, $\mu > 0$ including contours corresponding to the most important observables. The region preferred by a_μ at the 2σ and 1σ level is shown as the medium pink band and thin black dashed lines. The Higgs boson mass bound $M_h > 114$ GeV is satisfied to the right of the near-vertical dot-dashed red line at $m_{1/2} \approx 400$ GeV, and to the right of the black dashed line at $m_{1/2} \approx 150$ GeV $m_{\chi^\pm} > 104$ GeV. The plot displays clearly the tension between M_h , which is increased by larger $m_{1/2}$, and a_μ , which prefers smaller SUSY masses, but there is a non-vanishing region where both constraints are satisfied. For larger $\tan\beta$ this overlap region grows.

The small green region around $m_{1/2} \approx 100$ GeV is excluded by the decay $b \rightarrow s\gamma$. As mentioned before, the good agreement between SM theory and experiment favours destructive interference between the various SUSY contributions. In mSUGRA, the dominant contributions are the ones with charged Higgs or chargino exchange, and destructive interference requires $\mu A_t < 0$. Since mSUGRA predicts $A_t < 0$ almost independently of A_0 , positive μ is preferred by $b \rightarrow s\gamma$. It is a non-trivial success of mSUGRA that both a_μ and $b \rightarrow s\gamma$ prefer the same sign of μ , and this is the reason why the green region in figure 15 (a) is so small. However, for larger $\tan\beta$ the $b \rightarrow s\gamma$ -constraint excludes a larger part of the mSUGRA parameter space, and this counterbalances the preference of M_h and a_μ for larger $\tan\beta$. Contours for the decay $B_s \rightarrow \mu^+\mu^-$ are not shown in figure 15, but for large $\tan\beta \approx 50$ this decay becomes relevant, too. The current CDF limit (90) already begins to constrain the mSUGRA parameter space [88, 133].

The constraint imposed by the requirement that the lightest neutralino relic density coincides with the cold dark matter density preferred by WMAP [111] at the 2σ level is shown by the light turquoise band. This band is very narrow and thus allows to fix e.g. m_0 as a function of $m_{1/2}$. But since the relic density band is essentially orthogonal to the other regions it is possible to satisfy all constraints simultaneously.

All observables considered in figure 15 (a) have been combined with the electroweak precision observables M_W and $\sin^2\theta_{\text{eff}}$ in [119, 120]. In these references, χ^2 fits within mSUGRA have been performed, and remarkably there are mSUGRA parameter points that are consistent with all constraints. Figure 15 (b) shows an example of the total χ^2 as a function of $m_{1/2}$ for $\tan\beta = 10$ and various values of A_0 (m_0 is always fixed by the relic density constraint). The minimum $\chi_{\text{tot}}^2 = 2.55$ is obtained for $A_0 = m_{1/2} = 320$ GeV.

In fact, a similarly good fit quality with a $\chi_{\text{tot}}^2 < 3$ can be achieved for all values of $\tan\beta$ between 10 and 50, and the preferred mass range for $m_{1/2}$ is always between 300 and 600 GeV. For lower $\tan\beta$, the M_h - and a_μ -constraint are difficult to reconcile. For higher $\tan\beta$, $b \rightarrow s\gamma$ is a serious constraint. It should be noted that the significance of these tensions has grown recently since the experimental value of the top quark mass has gone down [120, 131]. Nevertheless, the fact that mSUGRA fits well to all observables and that the preferred mass range $m_{1/2} = 300 \dots 600$ GeV is rather low is very encouraging also in view of forthcoming SUSY searches at colliders.

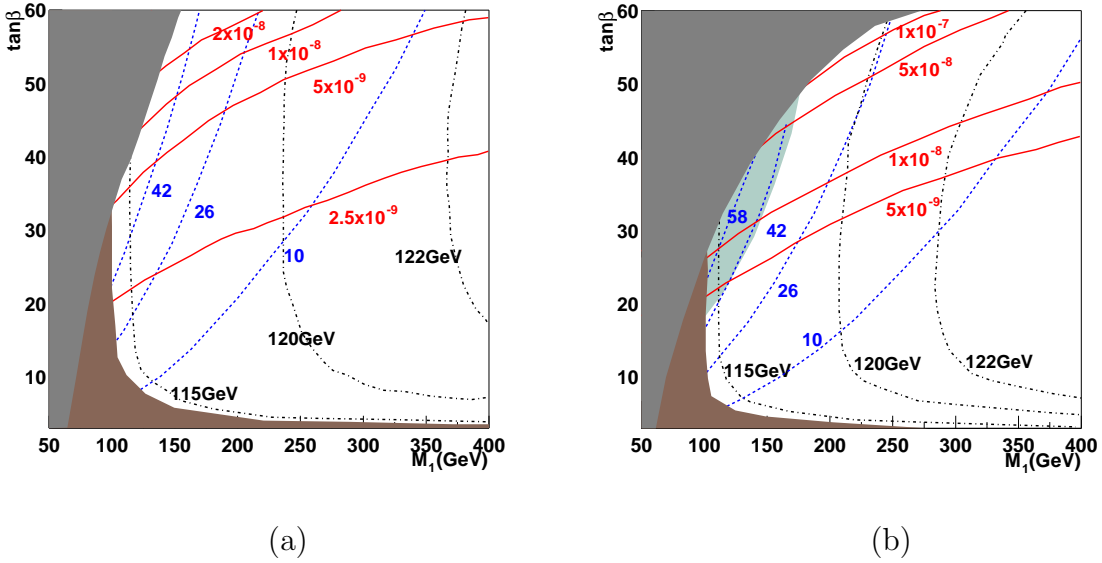


Figure 16. The M_1 - $\tan\beta$ plane in GMSB for $\mu > 0$ and for (a) $M_{\text{mess}} = 10^6$ GeV, $N_{\text{mess}} = 1$ and (b) $M_{\text{mess}} = 10^{15}$ GeV, $N_{\text{mess}} = 5$, taken from [133]. The shown contours correspond to $a_\mu \times 10^{10} = 10, 26, 42, 58$ (blue, dashed), to $\text{BR}(B_s \rightarrow \mu^+ \mu^-)$ (red, solid), and to M_h (black, dot-dashed). The light green region visible only in panel (b) is excluded by $b \rightarrow s\gamma$. The grey and dark brown regions are excluded by mass bounds on SUSY particles and the lightest Higgs boson.

4.4. Gauge-mediated SUSY breaking

Gauge-mediated SUSY breaking (GMSB) assumes that supersymmetry breaking is mediated from a hidden sector to the observable sector by gauge fields. In the simplest case there is an integer number N_{mess} of such messenger gauge fields, and these gauge fields have mass M_{mess} and form vector like $\mathbf{5} + \bar{\mathbf{5}}$ representations of SU(5). A major advantage of GMSB over the mSUGRA framework is that flavour universality naturally follows from the symmetries of the messenger interactions (see [134] for a review of GMSB).

The low-energy properties of GMSB are described by the following parameters:

$$M_{\text{mess}}, N_{\text{mess}}, \Lambda, \tan\beta, \text{sign}(\mu), \quad (94)$$

where the mass scale Λ is related to the SUSY breaking scale \sqrt{F} by $\Lambda = F/M_{\text{mess}}$. Λ determines the overall scale of the soft breaking parameters and can be traded for one of them, e.g. M_1 . At M_{mess} boundary conditions are imposed on the MSSM soft parameters, and renormalization group running is used to determine the MSSM spectrum at the electroweak scale.

The GMSB predictions for a_μ and related observables have been studied in [72, 135–137] and compared to the predictions of mSUGRA and other models in [47, 80, 133]. Figure 16 from [133] shows two contour plots in the M_1 - $\tan\beta$ plane for $\mu > 0$ and for $M_{\text{mess}} = 10^6$ GeV, $N_{\text{mess}} = 1$ and $M_{\text{mess}} = 10^{15}$ GeV, $N_{\text{mess}} = 5$. In both

cases, the experimental result for a_μ can be easily accommodated by GMSB. For any given M_1 and $\tan\beta$, a_μ is larger in panel (b) mainly due to the relative suppression of the sfermion masses by $1/\sqrt{N_{\text{mess}}}$. However, curiously due to the other constraints the highest values for a_μ^{SUSY} can be obtained for smaller N_{mess} [47].

Like in mSUGRA a_μ and $b \rightarrow s\gamma$ both favour the same, positive sign of μ . Moreover, in GMSB both stops and charged Higgs bosons are typically rather heavy, especially for small M_{mess} . As a result, GMSB is not very significantly constrained by the b -decays [133]. Conversely, observation of non-standard effects in b -decays would seriously constrain GMSB models.

4.5. Anomaly-mediated SUSY breaking

In anomaly-mediated SUSY breaking (AMSB) SUSY breaking takes place in a hidden sector and is transmitted to the observable sector via the anomalous breaking of superconformal (or super-Weyl) invariance [138, 139]. In this scenario the gaugino and scalar mass soft parameters are related to the breaking of scale invariance, expressed in terms of the gauge β functions and the anomalous dimensions of the matter fields. Most notably, the AMSB contributions to the gaugino masses are $M_i \propto -b_i\alpha_i$ with the one-loop coefficients $(b_i) = (3, -1, -33/5)$ of the SU(3), SU(2) and U(1) β functions. While these AMSB contributions to the soft SUSY breaking terms are always present in hidden sector models, they are usually subdominant. In the absence of any larger contributions, AMSB leads to a very predictive framework that is qualitatively very different from mSUGRA or GMSB.

The parameters of minimal AMSB (mAMSB) are

$$M_{\text{aux}}, m_0, \tan\beta, \text{sign}(\mu). \quad (95)$$

M_{aux} is a common scale for all soft parameters, and m_0 is a universal additional scalar mass term that does not originate from the super-Weyl anomaly. This term is necessary in order to avoid tachyonic sleptons.

A crucial feature of AMSB is that the signs of M_3 and A_t (in the convention that $M_2 > 0$) are reversed compared to the mSUGRA and GMSB cases. As a result, the $b \rightarrow s\gamma$ constraint favours negative μ and thus negative a_μ^{SUSY} . If the observed deviation of the experimental from the SM theory value of a_μ would have turned out to have a negative sign, AMSB would be favoured over virtually all other models of SUSY breaking [140, 141]. However, since the deviation is positive AMSB is disfavoured compared to other scenarios such as mSUGRA or GMSB [65]. This clearly shows how combining information on low-energy physics can discriminate between different well-motivated SUSY breaking mechanisms.

Figure 17 shows an example from [133] of the m_0 - $\tan\beta$ plane of mAMSB for $M_{\text{aux}} = 50$ TeV and $\mu > 0$. The region for $\tan\beta > 30$ is almost entirely excluded by the $b \rightarrow s\gamma$ constraint (light green). For low $\tan\beta$, the Higgs boson mass bound and a_μ restrict the parameter space. Nevertheless, for moderate values of $\tan\beta$ and m_0 it is possible to consistently accommodate b -decays, a_μ and M_h within mAMSB.

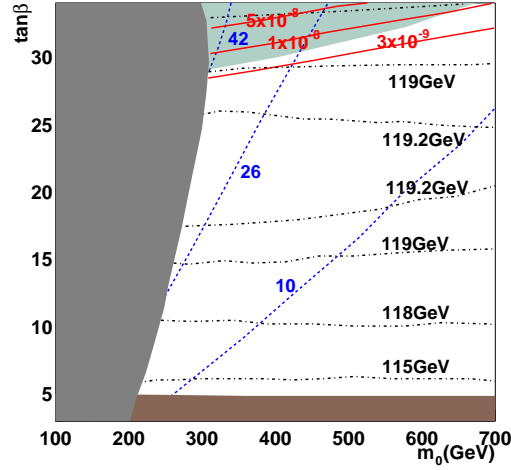


Figure 17. The m_0 - $\tan\beta$ plane in mAMSb for $\mu > 0$ and $M_{\text{aux}} = 50$ TeV, taken from [133]. The shown contours correspond to $a_\mu \times 10^{10} = 10, 26, 42$ (blue, dashed), to $\text{BR}(B_s \rightarrow \mu^+ \mu^-)$ (red, solid), and to M_h (black, dot-dashed). The light green region is excluded by $b \rightarrow s\gamma$. They grey and dark brown regions are excluded by mass bounds on SUSY particles and the lightest Higgs boson.

4.6. MSSM parameter scan

In this subsection we present a general, model-independent MSSM parameter scan that summarizes the current status of a_μ in SUSY. This scan shows the maximum results for a_μ in the MSSM if all parameters are independently varied and the range of SUSY masses for which the MSSM can accommodate the experimental result. The full set of one- and two-loop contributions in (79) are taken into account, and the results are compared with the current deviation between the experimental and SM result (5). The scan can be viewed as an update of the one presented in [65].

The MSSM parameters have been varied in the ranges

$$|\mu|, M_2, m_{L,\tilde{f}}, m_{R,\tilde{f}}, |A_f| \leq 3000 \text{ GeV}, \quad M_A = 90 \dots 3000 \text{ GeV}, \quad \tan\beta = 50, \quad (96)$$

where the upper limit is motivated by naturalness arguments, and the lower limit on M_A corresponds to the experimental limit. The parameter $\tan\beta$ has not been varied because the essentially linear $\tan\beta$ dependence of a_μ^{SUSY} has been sufficiently established before. All other parameters have been varied independently, except that M_1 has been fixed via the GUT relation, $A_\mu = 0$, $m_{L,\tilde{b}} = m_{L,\tilde{\tau}}$, $m_{R,\tilde{b}} = m_{R,\tilde{\tau}}$ and $A_b = A_\tau$. These constraints do not have much impact on the maximum contributions [65]. The 3rd generation sfermion parameters are significantly restricted by experimental constraints on M_h , $\Delta\rho$ and b -decays. Only parameter points have been considered that are in agreement with these constraints, according to the same criteria as in the “weak bounds” of [48]. Note that the precise values used in these constraints have not much influence on the maximum

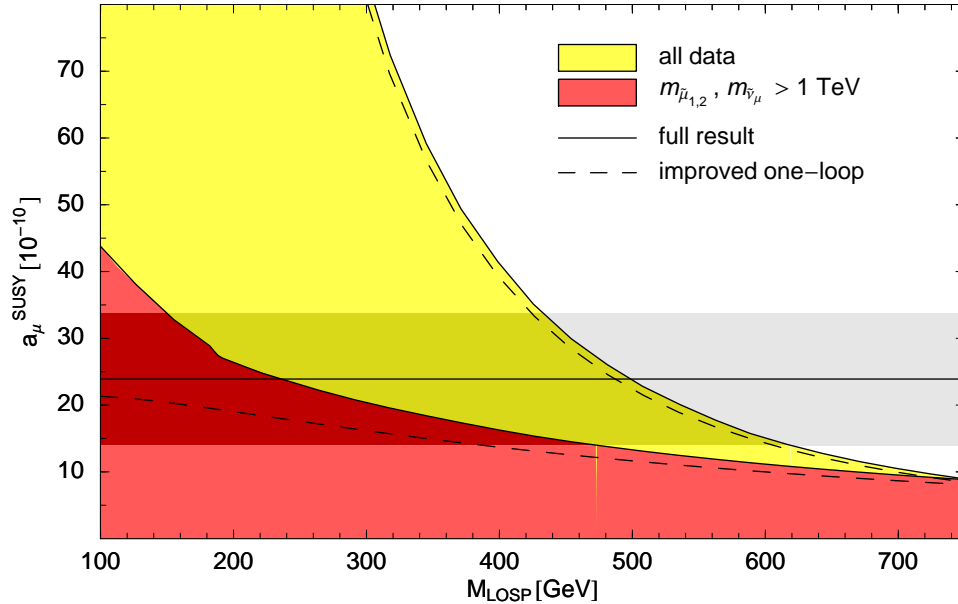


Figure 18. Allowed values of a_μ^{SUSY} as a function of the mass of the lightest observable supersymmetric particle $M_{\text{LOSP}} = \min(m_{\tilde{\chi}_1^\pm}, m_{\tilde{\chi}_2^0}, m_{\tilde{f}_i})$, from a scan of the MSSM parameter space in the range (96) and for $\tan\beta = 50$. The 1σ region corresponding to the deviation between experimental and SM values (5) is indicated. The light yellow region corresponds to all data points that satisfy the experimental constraints from b -decays, M_h and $\Delta\rho$. In the red region, the smuons and sneutrinos are heavier than 1 TeV. The dashed lines correspond to the contours that arise from ignoring the two-loop corrections from chargino/neutralino- and sfermion-loop diagrams.

results in figure 18 as they affect essentially only the two-loop sfermion contributions.

Figure 18 shows the results of the scan. The light yellow region corresponds to the possible results for a_μ^{SUSY} , given by (79), as a function of M_{LOSP} , if all parameters are varied in the range (96). The red region corresponds to the situation that the smuons and sneutrinos are heavy,

$$m_{\tilde{\mu}_{1,2}}, m_{\tilde{\nu}_\mu} > 1000 \text{ GeV}, \quad (97)$$

while charginos, neutralinos and stops and sbottoms can still be light. A dedicated analysis of this situation is of interest since heavy 1st and 2nd generation sfermions are sometimes considered as a possible explanation of the absence of observable SUSY contributions to flavour-changing neutral currents and CP-violating observables.

The dashed lines in figure 18 correspond to the results if the genuine two-loop diagrams are neglected and only the one-loop contributions and the logarithmic QED-corrections (78) are taken into account.

The yellow region corresponds to all data points and thus to the maximum possible values of a_μ^{SUSY} compatible with the parameter range (96) and the experimental constraints from b -decays, M_h and $\Delta\rho$. The SUSY contributions can accommodate the observed result (5) within 1σ for LOSP masses below about 600 GeV. For LOSP masses below about 440 GeV, the SUSY contributions can be even too large, and thus the a_μ -

measurement significantly restricts the MSSM parameter space in this low-mass region.

The red region of figure 18 shows that heavy smuons and sneutrinos significantly suppress the maximum SUSY contributions to a_μ . Nevertheless, the contributions can be in the 1σ region (5) for M_{LOSP} between about 150 and 470 GeV.

We close the section with a couple of instructive but more technical remarks. On the one hand we analyze which parameter regions give rise to the maximum contributions found in figure 18. On the other hand we explain the reasons for the different behaviour of the two-loop contributions in the red and yellow regions.

In the yellow region, corresponding to all data points, the maximum values are obtained for $\mu = 3000$ GeV, the upper border of the allowed range, and for $M_2 \approx m_{L,R,\bar{\mu}}$. The reason is that the one-loop bino-exchange diagram (N1) of figure 2 is linear in μ and therefore dominant for large μ . In comparing our results with the ones of [65], one should note that since the maximum contributions are obtained at the border of the allowed multi-dimensional parameter region, an unbiased random generation of parameter points as the one used in [65] has difficulties in finding the maximum contributions. Therefore the results displayed in figure 1 and equation (3) of [65] slightly underestimate the maximum contributions allowed by the employed parameter ranges. Since the maximum contributions are obtained for large μ , the two-loop chargino/neutralino contributions are negligible, but the two-loop sfermion contributions shift the contour by about 5%. Another consequence of the dominance of diagram (N1) is that the border of the yellow contour scales linearly with the maximum value for μ used in scanning over the SUSY parameters.

The one-loop contributions in the red region are maximized for smuon masses of 1 TeV and $\mu = M_2$. Since therefore μ , M_2 and M_A can be simultaneously small, substantial two-loop chargino/neutralino contributions are possible. Furthermore, the two-loop sfermion contributions can be large as well since the stop and sbottom mass parameters are not required to be universal. The largest results in the red region are obtained if both $m_{L,\bar{b}}$ and $m_{R,\bar{b}}$ are small but $m_{R,\bar{t}}$ is large. In this situation, the sbottom-loop contribution can be larger than the results displayed in figure 11 without any violation of the experimental constraints on M_h , $\Delta\rho$ or b -decays.

The significance of the two-loop corrections in the red region is reflected in the fact that the contour shifts by more than 30% in the low-mass region if the two-loop corrections are neglected.

5. Concluding remarks and outlook

The final result of the Brookhaven $a_\mu = (g_\mu - 2)/2$ measurement shows a deviation of $23.9(9.9) \times 10^{-10}$, corresponding to 2 ppm and more than 2σ , from the corresponding SM prediction based on e^+e^- data. The Brookhaven experiment is the first magnetic dipole moment measurement that is sensitive to physics at the electroweak scale, just like the previous CERN experiment was the first to be sensitive to hadronic effects. But unlike the CERN experiment, which confirmed the SM prediction of the hadronic

effects, the Brookhaven experiment would prefer electroweak effects that are about 2.5 times larger than predicted by the SM.

The SUSY contributions to a_μ are essentially proportional to $\tan\beta \text{sign}(\mu)/M_{\text{SUSY}}^2$. Hence for moderate or large $\tan\beta$ these contributions can easily be larger than the electroweak SM contributions and thus constitute the origin of the discrepancy between the experiment and the SM prediction. Furthermore, in this case a_μ strongly favours positive μ , which is a very important piece of information for SUSY phenomenology. The qualitative behaviour of a_μ^{SUSY} can be well understood using the mass insertion technique. The $\tan\beta$ -enhancement arises in diagrams where the necessary chirality flip occurs at a muon Yukawa coupling, either to a Higgsino or Higgs boson, because this coupling is enhanced by $1/\cos\beta \approx \tan\beta$ compared to its SM value. The μ -parameter mediates the transition between the two Higgs/Higgsino doublets $H_{1,2}$, and this transition enhances diagrams because only H_1 couples to muons while H_2 has the larger vacuum expectation value.

For a quantitative analysis, the MSSM prediction of a_μ has to be known with an accuracy that matches the one of the SM prediction. This goal has been achieved with the calculation of the full one-loop and leading two-loop contributions, as given in (79). Since the remaining theory uncertainty is dominated by one particular class of unknown two-loop diagrams, an even more satisfactory MSSM prediction could be obtained by evaluating this missing class of diagrams.

If supersymmetry is assumed to exist, many non-trivial details about the SUSY spectrum can be derived from a_μ . For example, for $\tan\beta = 10$ four SUSY particles must be lighter than 500(1000) GeV at the $1\sigma(2\sigma)$ level. And even in a very conservative interpretation, where a 5σ deviation in a_μ is tolerated, significant lower bounds on the SUSY masses can be derived in a model-independent way. These bounds cannot be obtained from any other observable and establish a_μ as one of the most important indirect probes of SUSY.

There are several other observables that are relevant for SUSY phenomenology and provide constraints on SUSY parameters, although a_μ is unique in its largest discrepancy between experimental and SM values. On a qualitative level, the relation between a_μ and these other observables is the following. a_μ favours rather large $\tan\beta$ and/or small SUSY masses and positive μ . If neutralinos constitute a component of dark matter, the dark matter detection rate is enhanced by large $\tan\beta$ and positive μ . Therefore, the a_μ result is encouraging for future dark matter detection experiments.

The preference of a_μ for rather light SUSY masses is supported by the experimental results for the electroweak precision observables M_W and $\sin^2\theta_{\text{eff}}$, which favour small but non-zero SUSY contributions. The preference of a_μ for not too small $\tan\beta$ is supported by the constraint derived from the lower bound on M_h . However, the bound on M_h also favours large SUSY masses (particularly stop masses) over light ones. Furthermore, the MSSM parameter space for large $\tan\beta$ is significantly constrained by the rare b -decays $b \rightarrow s\gamma$ and $B_s \rightarrow \mu^+\mu^-$. The decay $b \rightarrow s\gamma$ shows a similar dependence on $\text{sign}(\mu)$ as a_μ . This already constitutes a crucial test of minimal models. For instance, in mSUGRA

or GMSB, but not in AMSB, a_μ and $b \rightarrow s\gamma$ favour the same sign of μ .

Given the tension between all these observables it is non-trivial that all constraints can be simultaneously satisfied, even in the simplest but well-motivated models such as mSUGRA or GMSB. Mainly driven by a_μ , the parameter points satisfying all constraints prefer a number of (though not necessarily all) SUSY particles to be light. This result is clearly encouraging for the SUSY search at the LHC and the ILC.

We have summarized the current status of a_μ and SUSY in figure 18, which shows the possible values of a_μ^{SUSY} , compared with the observed deviation between experiment and the SM prediction. The MSSM parameters have been scanned over in the range allowed by all relevant constraints from other collider experiments, and in the evaluation of a_μ^{SUSY} all known one- and two-loop contributions have been taken into account. The result confirms again that SUSY can accommodate the a_μ result consistently with all other constraints and that the preferred mass range is rather low. On a more technical level, the figure also shows that two-loop SUSY effects can be important.

In spite of the impressive current status, progress on a_μ is important and will come both from the experimental and the theoretical side. Already a small improvement of the precision could be sufficient to increase the discrepancy between the experimental and SM values of a_μ to 4–5 σ and thus to establish the existence of non-SM contributions. Currently the SM theory prediction has a larger uncertainty than the experimental value, and within the SM prediction the main uncertainty is related to the hadronic vacuum polarization. However, this uncertainty can be expected to be significantly reduced as a result of ongoing measurements of $e^+e^- \rightarrow \text{hadrons}$ by CMD2 and SND in Novosibirsk and, using radiative return, by B factories and KLOE. Another important source of theoretical uncertainty is related to the hadronic light-by-light scattering contribution. It is a very challenging theoretical task to evaluate this contribution, and current error estimates vary between $2.5 \dots 4 \times 10^{-10}$. However, further progress in the understanding of this contribution can be expected, and one can hope that the full SM theory uncertainty can be reduced to below 4×10^{-10} in the foreseeable future [17]. Finally, progress can be expected from the experimental determination of a_μ . Since the current measurement precision is statistics limited, a new experiment using similar methods with only straightforward improvements could reduce the uncertainty by a factor of 2.5 or more, and an according plan has already been outlined [6, 142].

After more than 40 years of experimental and theoretical progress, the observable a_μ has become a sensitive probe of physics at the electroweak scale. Already today it is one of the most important constraints of physics beyond the SM. In the near future, particle physics will enter a new era where the detailed structure of physics at the electroweak scale and above will be unravelled by experiments at the LHC and possibly later the ILC. Not only new particles like smuons or charginos might be discovered, but also the other indirect constraints from the observables mentioned above will become more stringent. The magnetic moment of the muon will provide a crucial cross-check and complement of the forthcoming experiments.

Acknowledgments

It is a pleasure to thank A. Martin for the invitation to write this review and S. Heinemeyer, W. Hollik, J. Illana, S. Rigolin and G. Weiglein for discussions and collaborations. Furthermore, I am grateful to A. Arhrib, W.-F. Chang, A. Czarnecki, A. Dedes, T. Jones, S. Martin, K. Matchev, T. Moroi, A. Nyffeler, M. J. Ramsey-Musolf and T. Teubner for discussions on various aspects of the muon magnetic moment and to C. Fischer, S. Heinemeyer, T. Plehn and H. Stöckinger-Kim for critical comments on the manuscript.

References

- [1] R. M. Carey *et al.*, “New measurement of the anomalous magnetic moment of the positive muon,” *Phys. Rev. Lett.* **82** (1999) 1632.
- [2] H. N. Brown *et al.* [Muon (g-2) Collaboration], “Improved measurement of the positive muon anomalous magnetic moment,” *Phys. Rev. D* **62**, 091101 (2000) [arXiv:hep-ex/0009029].
- [3] H. N. Brown *et al.* [Muon g-2 Collaboration], “Precise measurement of the positive muon anomalous magnetic moment,” *Phys. Rev. Lett.* **86**, 2227 (2001) [arXiv:hep-ex/0102017].
- [4] G. W. Bennett *et al.* [Muon g-2 Collaboration], “Measurement of the negative muon anomalous magnetic moment to 0.7-ppm,” *Phys. Rev. Lett.* **92** (2004) 161802 [arXiv:hep-ex/0401008].
- [5] G. W. Bennett *et al.* [Muon g-2 Collaboration], “Measurement of the positive muon anomalous magnetic moment to 0.7-ppm,” *Phys. Rev. Lett.* **89** (2002) 101804 [Erratum-ibid. **89** (2002) 129903] [arXiv:hep-ex/0208001].
- [6] G. W. Bennett [Muon Collaboration], “Final report of the muon E821 anomalous magnetic moment measurement at BNL,” *Phys. Rev. D* **73** (2006) 072003 [arXiv:hep-ex/0602035].
- [7] J. S. Schwinger, “On Quantum Electrodynamics And The Magnetic Moment Of The Electron,” *Phys. Rev.* **73** (1948) 416.
- [8] W. J. Marciano and B. L. Roberts, “Status of the hadronic contribution to the muon (g-2) value,” arXiv:hep-ph/0105056.
- [9] K. Melnikov, “On the theoretical uncertainties in the muon anomalous magnetic moment,” *Int. J. Mod. Phys. A* **16**, 4591 (2001) [arXiv:hep-ph/0105267].
- [10] M. Knecht, “The anomalous magnetic moment of the muon: A theoretical introduction,” *Lect. Notes Phys.* **629** (2004) 37 [arXiv:hep-ph/0307239].
- [11] M. Davier and W. J. Marciano, “The theoretical prediction for the muon anomalous magnetic moment,” *Ann. Rev. Nucl. Part. Sci.* **54** (2004) 115.
- [12] M. Passera, “The standard model prediction of the muon anomalous magnetic moment,” *J. Phys. G* **31** (2005) R75 [arXiv:hep-ph/0411168].
- [13] M. Knecht and A. Nyffeler, “Hadronic light-by-light corrections to the muon g-2: The pion-pole contribution,” *Phys. Rev. D* **65**, 073034 (2002) [arXiv:hep-ph/0111058].
- [14] M. Knecht, A. Nyffeler, M. Perrottet and E. De Rafael, “Hadronic light-by-light scattering contribution to the muon g-2: An effective field theory approach,” *Phys. Rev. Lett.* **88**, 071802 (2002) [arXiv:hep-ph/0111059].
- [15] M. Davier, S. Eidelman, A. Hocker and Z. Zhang, “Updated estimate of the muon magnetic moment using revised results from e+ e- annihilation,” *Eur. Phys. J. C* **31** (2003) 503 [arXiv:hep-ph/0308213].
- [16] K. Melnikov and A. Vainshtein, “Hadronic light-by-light scattering contribution to the muon anomalous magnetic moment revisited,” *Phys. Rev. D* **70** (2004) 113006 [arXiv:hep-ph/0312226].

- [17] K. Hagiwara, A. D. Martin, D. Nomura and T. Teubner, “Predictions for $g-2$ of the muon and $\alpha(\text{QED})(M_Z^2)$,” *Phys. Rev. D* **69** (2004) 093003 [arXiv:hep-ph/0312250].
- [18] J. F. de Troconiz and F. J. Yndurain, “The hadronic contributions to the anomalous magnetic moment of the muon,” *Phys. Rev. D* **71** (2005) 073008 [arXiv:hep-ph/0402285].
- [19] J. Bailey *et al.* [CERN-Mainz-Daresbury Collaboration], “Final Report On The Cern Muon Storage Ring Including The Anomalous Magnetic Moment And The Electric Dipole Moment Of The Muon, And A Direct Test Of Relativistic Time Dilation,” *Nucl. Phys. B* **150** (1979) 1.
- [20] A. Czarnecki and W. J. Marciano, “The muon anomalous magnetic moment: A harbinger for ‘new physics’,” *Phys. Rev. D* **64** (2001) 013014 [arXiv:hep-ph/0102122].
- [21] H. P. Nilles, “Supersymmetry, Supergravity And Particle Physics,” *Phys. Rept.* **110** (1984) 1.
- [22] H. E. Haber and G. L. Kane, “The Search For Supersymmetry: Probing Physics Beyond The Standard Model,” *Phys. Rept.* **117** (1985) 75.
- [23] S. P. Martin, “A supersymmetry primer,” arXiv:hep-ph/9709356.
- [24] D. J. H. Chung, L. L. Everett, G. L. Kane, S. F. King, J. D. Lykken and L. T. Wang, “The soft supersymmetry-breaking Lagrangian: Theory and applications,” *Phys. Rept.* **407** (2005) 1 [arXiv:hep-ph/0312378].
- [25] I. J. R. Aitchison, “Supersymmetry and the MSSM: An elementary introduction,” arXiv:hep-ph/0505105.
- [26] W. Hollik, E. Kraus, M. Roth, C. Rupp, K. Sibold and D. Stöckinger, “Renormalization of the minimal supersymmetric standard model,” *Nucl. Phys. B* **639**, 3 (2002) [arXiv:hep-ph/0204350].
- [27] S. Heinemeyer, W. Hollik and G. Weiglein, “Electroweak precision observables in the minimal supersymmetric standard model,” *Phys. Rept.* **425** (2006) 265 [arXiv:hep-ph/0412214].
- [28] B. Ananthanarayan, G. Lazarides and Q. Shafi, “Top mass prediction from supersymmetric guts,” *Phys. Rev. D* **44**, 1613 (1991).
- [29] R. Z. Roskies, M. J. Levine and E. Remiddi, “Analytic Evaluation Of Sixth Order Contributions To The Electron’s G Factor,” in *Quantum Electrodynamics*, ed. T. Kinoshita (World Scientific, Singapore, 1990).
- [30] A. Czarnecki and B. Krause, “Electroweak corrections to the muon anomalous magnetic moment,” *Nucl. Phys. Proc. Suppl.* **51C** (1996) 148 [arXiv:hep-ph/9606393].
- [31] S. Ferrara and E. Remiddi, “Absence Of The Anomalous Magnetic Moment In A Supersymmetric Abelian Gauge Theory,” *Phys. Lett. B* **53** (1974) 347.
- [32] S. Ferrara and M. Porrati, “Supersymmetric sum rules on magnetic dipole moments of arbitrary spin particles,” *Phys. Lett. B* **288** (1992) 85.
- [33] P. Fayet, in *Unification of the Fundamental Particles Interactions*, ed. S. Ferrara, J. Ellis, and P. van Nieuwenhuizen (Plenum, New York, 1980), p. 587.
- [34] J. A. Grifols and A. Mendez, “Constraints On Supersymmetric Particle Masses From $(G-2)$ Mu,” *Phys. Rev. D* **26**, 1809 (1982).
- [35] J. R. Ellis, J. S. Hagelin and D. V. Nanopoulos, “Spin 0 Leptons And The Anomalous Magnetic Moment Of The Muon,” *Phys. Lett. B* **116** (1982) 283.
- [36] R. Barbieri and L. Maiani, “The Muon Anomalous Magnetic Moment In Broken Supersymmetric Theories,” *Phys. Lett. B* **117**, 203 (1982).
- [37] D. A. Kosower, L. M. Krauss and N. Sakai, “Low-Energy Supergravity And The Anomalous Magnetic Moment Of The Muon,” *Phys. Lett. B* **133**, 305 (1983).
- [38] T. C. Yuan, R. Arnowitt, A. H. Chamseddine and P. Nath, “Supersymmetric Electroweak Effects On $G-2$ (Mu),” *Z. Phys. C* **26**, 407 (1984).
- [39] J. C. Romao, A. Barroso, M. C. Bento and G. C. Branco, “Flavor Violation In Supersymmetric Theories,” *Nucl. Phys. B* **250**, 295 (1985).
- [40] I. Vendramin, “Constraints On Supersymmetric Parameters From Muon Magnetic Moment,” *Nuovo Cim. A* **101** (1989) 731.
- [41] S. A. Abel, W. N. Cottingham and I. B. Whittingham, “The Muon Magnetic Moment In Flipped

- SU(5),” *Phys. Lett. B* **259** (1991) 307.
- [42] J. L. Lopez, D. V. Nanopoulos and X. Wang, “Large $(g-2)_\mu$ in SU(5) \times U(1) supergravity models,” *Phys. Rev. D* **49**, 366 (1994) [arXiv:hep-ph/9308336].
- [43] U. Chattopadhyay and P. Nath, “Probing supergravity grand unification in the Brookhaven $g-2$ experiment,” *Phys. Rev. D* **53**, 1648 (1996) [arXiv:hep-ph/9507386].
- [44] T. Moroi, “The Muon Anomalous Magnetic Dipole Moment in the Minimal Supersymmetric Standard Model,” *Phys. Rev. D* **53** (1996) 6565 [Erratum-ibid. **56** (1997) 4424], hep-ph/9512396.
- [45] W. Hollik, J. I. Illana, S. Rigolin and D. Stöckinger, “One-loop MSSM contribution to the weak magnetic dipole moments of heavy fermions,” *Phys. Lett. B* **416** (1998) 345 [arXiv:hep-ph/9707437].
- [46] W. Hollik, J. I. Illana, S. Rigolin and D. Stöckinger, “Weak electric dipole moments of heavy fermions in the MSSM,” *Phys. Lett. B* **425** (1998) 322 [arXiv:hep-ph/9711322].
- [47] S. Martin and J. Wells, “Muon anomalous magnetic dipole moment in supersymmetric theories,” *Phys. Rev. D* **64** (2001) 035003, hep-ph/0103067.
- [48] S. Heinemeyer, D. Stöckinger and G. Weiglein, “Two-loop SUSY corrections to the anomalous magnetic moment of the muon,” *Nucl. Phys. B* **690** (2004) 62 [arXiv:hep-ph/0312264].
- [49] S. Heinemeyer, D. Stöckinger and G. Weiglein, “Electroweak and supersymmetric two-loop corrections to $(g-2)_\mu$,” *Nucl. Phys. B* **699** (2004) 103 [arXiv:hep-ph/0405255].
- [50] G. Degrossi and G. F. Giudice, “QED logarithms in the electroweak corrections to the muon anomalous magnetic moment,” *Phys. Rev. D* **58** (1998) 053007 [arXiv:hep-ph/9803384].
- [51] V. Smirnov, *Applied Asymptotic Expansions in Momenta and Masses*, Springer Verlag, Berlin (2002).
- [52] K. I. Aoki, Z. Hioki, M. Konuma, R. Kawabe and T. Muta, “Electroweak Theory. Framework Of On-Shell Renormalization And Study Of Higher Order Effects,” *Prog. Theor. Phys. Suppl.* **73**, 1 (1982).
- [53] M. Böhm, H. Spiesberger and W. Hollik, “On The One Loop Renormalization Of The Electroweak Standard Model And Its Application To Leptonic Processes,” *Fortsch. Phys.* **34**, 687 (1986).
- [54] S. M. Barr and A. Zee, “Electric Dipole Moment Of The Electron And Of The Neutron,” *Phys. Rev. Lett.* **65** (1990) 21 [Erratum-ibid. **65** (1990) 2920].
- [55] D. Chang, W. Y. Keung and A. Pilaftsis, “New two-loop contribution to electric dipole moment in supersymmetric theories,” *Phys. Rev. Lett.* **82** (1999) 900 [Erratum-ibid. **83** (1999) 3972] [arXiv:hep-ph/9811202].
- [56] A. Pilaftsis, “Higgs-boson two-loop contributions to electric dipole moments in the MSSM,” *Phys. Lett. B* **471** (1999) 174 [arXiv:hep-ph/9909485].
- [57] D. Chang, W. F. Chang, C. H. Chou and W. Y. Keung, “Large two-loop contributions to $g-2$ from a generic pseudoscalar boson,” *Phys. Rev. D* **63** (2001) 091301 [arXiv:hep-ph/0009292].
- [58] K. m. Cheung, C. H. Chou and O. C. W. Kong, “Muon anomalous magnetic moment, two-Higgs-doublet model, and supersymmetry,” *Phys. Rev. D* **64** (2001) 111301 [arXiv:hep-ph/0103183].
- [59] A. Arhrib and S. Baek, “Two-loop Barr-Zee type contributions to $(g-2)_\mu$ in the MSSM,” *Phys. Rev. D* **65** (2002) 075002 [arXiv:hep-ph/0104225].
- [60] C. H. Chen and C. Q. Geng, “The muon anomalous magnetic moment from a generic charged Higgs with SUSY,” *Phys. Lett. B* **511** (2001) 77 [arXiv:hep-ph/0104151].
- [61] A. Czarnecki, B. Krause and W. Marciano, “Electroweak Corrections To The Muon Anomalous Magnetic Moment,” *Phys. Rev. Lett.* **76** (1996) 3267, [arXiv:hep-ph/9512369].
- [62] T. Gribouk and A. Czarnecki, “Electroweak Interactions And The Muon $G-2$: Bosonic Two-Loop Effects,” *Phys. Rev. D* **72** (2005) 053016 [arXiv:hep-ph/0509205].
- [63] T. F. Feng, X. Q. Li, L. Lin, J. Maalampi and H. S. Song, “The two-loop supersymmetric corrections to lepton anomalous magnetic and electric dipole moments,” arXiv:hep-ph/0604171.
- [64] B. C. Allanach *et al.*, “The Snowmass points and slopes: Benchmarks for SUSY searches,” in *Proc. of the APS/DPF/DPB Summer Study on the Future of Particle Physics (Snowmass 2001)* ed.

- N. Graf, *Eur. Phys. J. C* **25** (2002) 113 [eConf **C010630** (2001) P125] [arXiv:hep-ph/0202233].
- [65] J. L. Feng and K. T. Matchev, “Supersymmetry and the anomalous magnetic moment of the muon,” *Phys. Rev. Lett.* **86**, 3480 (2001) [arXiv:hep-ph/0102146].
- [66] T. Ibrahim and P. Nath, “CP violation and the muon anomaly in $N = 1$ supergravity,” *Phys. Rev. D* **61** (2000) 095008 [arXiv:hep-ph/9907555].
- [67] T. Ibrahim and P. Nath, “Effects of large CP violating phases on $g(\mu)-2$ in MSSM,” *Phys. Rev. D* **62** (2000) 015004 [arXiv:hep-ph/9908443].
- [68] S. Heinemeyer, W. Hollik and G. Weiglein, “FeynHiggs: A program for the calculation of the masses of the neutral CP-even Higgs bosons in the MSSM,” *Comput. Phys. Commun.* **124** (2000) 76 [arXiv:hep-ph/9812320]. The codes are accessible via www.feynhiggs.de.
- [69] S. Heinemeyer, W. Hollik and G. Weiglein, “The masses of the neutral CP-even Higgs bosons in the MSSM: Accurate analysis at the two-loop level,” *Eur. Phys. J. C* **9** (1999) 343 [arXiv:hep-ph/9812472].
- [70] G. Degrandi, S. Heinemeyer, W. Hollik, P. Slavich and G. Weiglein, “Towards high-precision predictions for the MSSM Higgs sector,” *Eur. Phys. J. C* **28** (2003) 133 [arXiv:hep-ph/0212020].
- [71] T. Hahn, W. Hollik, S. Heinemeyer and G. Weiglein, “Precision Higgs masses with FeynHiggs 2.2,” arXiv:hep-ph/0507009.
- [72] M. Carena, G. F. Giudice and C. E. M. Wagner, “Constraints on supersymmetric models from the muon anomalous magnetic moment,” *Phys. Lett. B* **390** (1997) 234 [arXiv:hep-ph/9610233].
- [73] L. L. Everett, G. L. Kane, S. Rigolin and L. T. Wang, “Implications of muon $g-2$ for supersymmetry and for discovering superpartners directly,” *Phys. Rev. Lett.* **86** (2001) 3484 [arXiv:hep-ph/0102145].
- [74] U. Chattopadhyay and P. Nath, “Upper limits on sparticle masses from $g-2$ and the possibility for discovery of SUSY at colliders and in dark matter searches,” *Phys. Rev. Lett.* **86** (2001) 5854 [arXiv:hep-ph/0102157].
- [75] S. Komine, T. Moroi and M. Yamaguchi, “Recent result from E821 experiment on muon $g-2$ and unconstrained minimal supersymmetric standard model,” *Phys. Lett. B* **506** (2001) 93 [arXiv:hep-ph/0102204].
- [76] T. Ibrahim, U. Chattopadhyay and P. Nath, “Constraints on explicit CP violation from the Brookhaven muon $g-2$ experiment,” *Phys. Rev. D* **64** (2001) 016010 [arXiv:hep-ph/0102324].
- [77] J. R. Ellis, D. V. Nanopoulos and K. A. Olive, “Combining the muon anomalous magnetic moment with other constraints on the CMSSM,” *Phys. Lett. B* **508** (2001) 65 [arXiv:hep-ph/0102331].
- [78] R. Arnowitt, B. Dutta, B. Hu and Y. Santoso, “Muon $G-2$, Dark Matter Detection And Accelerator Physics,” *Phys. Lett. B* **505** (2001) 177 [arXiv:hep-ph/0102344].
- [79] K. Choi, K. Hwang, S. K. Kang, K. Y. Lee and W. Y. Song, “Probing the messenger of supersymmetry breaking by the muon anomalous magnetic moment,” *Phys. Rev. D* **64** (2001) 055001 [arXiv:hep-ph/0103048].
- [80] H. Baer, C. Balazs, J. Ferrandis and X. Tata, “Impact of muon anomalous magnetic moment on supersymmetric models,” *Phys. Rev. D* **64** (2001) 035004 [arXiv:hep-ph/0103280].
- [81] A. Djouadi, M. Drees and J. L. Kneur, “Constraints On The Minimal Supergravity Model And Prospects For Susy Particle Production At Future Linear $E+ E-$ Colliders,” *JHEP* **0108** (2001) 055 [arXiv:hep-ph/0107316].
- [82] E. A. Baltz and P. Gondolo, “Implications of muon anomalous magnetic moment for supersymmetric dark matter,” *Phys. Rev. Lett.* **86** (2001) 5004 [arXiv:hep-ph/0102147].
- [83] J. Hisano and K. Tobe, “Neutrino masses, muon $g-2$, and lepton-flavour violation in the supersymmetric see-saw model,” *Phys. Lett. B* **510**, 197 (2001) [arXiv:hep-ph/0102315].
- [84] Y. G. Kim and M. M. Nojiri, “Implications of muon anomalous magnetic moment for direct detection of neutralino dark matter,” *Prog. Theor. Phys.* **106** (2001) 561 [arXiv:hep-ph/0104258].
- [85] G. C. Cho and K. Hagiwara, “Supersymmetric contributions to muon $g-2$ and the electroweak precision measurements,” *Phys. Lett. B* **514** (2001) 123 [arXiv:hep-ph/0105037].

- [86] R. Arnowitt, B. Dutta and Y. Santoso, “Susy Phases, The Electron Electric Dipole Moment And The Muon Magnetic Moment,” *Phys. Rev. D* **64** (2001) 113010 [arXiv:hep-ph/0106089].
- [87] G. Belanger, F. Boudjema, A. Cottrant, R. M. Godbole and A. Semenov, “The MSSM invisible Higgs in the light of dark matter and g-2,” *Phys. Lett. B* **519** (2001) 93 [arXiv:hep-ph/0106275].
- [88] A. Dedes, H. K. Dreiner and U. Nierste, “Correlation of $B_s \rightarrow \mu^+ \mu^-$ and (g-2)(mu) in minimal supergravity,” *Phys. Rev. Lett.* **87** (2001) 251804 [arXiv:hep-ph/0108037].
- [89] S. Komine, T. Moroi and M. Yamaguchi, “No-scale scenarios in the light of new measurement of muon anomalous magnetic moment,” *Phys. Lett. B* **507** (2001) 224 [arXiv:hep-ph/0103182].
- [90] S. Baek, P. Ko and H. S. Lee, “Muon anomalous magnetic moment, $B \rightarrow X_s \gamma$ and dark matter detection in the string models with dilaton domination,” *Phys. Rev. D* **65**, 035004 (2002) [arXiv:hep-ph/0103218].
- [91] S. Baek, T. Goto, Y. Okada and K. i. Okumura, “Muon anomalous magnetic moment, lepton flavor violation, and flavor changing neutral current processes in SUSY GUT with right-handed neutrino,” *Phys. Rev. D* **64**, 095001 (2001) [arXiv:hep-ph/0104146].
- [92] K. Enqvist, E. Gabrielli and K. Huitu, “g-2 of the muon in SUSY models with gauge multiplets in the bulk of extra-dimensions,” *Phys. Lett. B* **512** (2001) 107 [arXiv:hep-ph/0104174].
- [93] D. G. Cerdeno, E. Gabrielli, S. Khalil, C. Munoz and E. Torrente-Lujan, “Muon anomalous magnetic moment in supersymmetric scenarios with an intermediate scale and nonuniversality,” *Phys. Rev. D* **64** (2001) 093012 [arXiv:hep-ph/0104242].
- [94] M. Graesser and S. D. Thomas, “Supersymmetric relations among electromagnetic dipole operators,” *Phys. Rev. D* **65**, 075012 (2002) [arXiv:hep-ph/0104254].
- [95] Z. Chacko and G. D. Kribs, “Constraints On Lepton Flavor Violation In The Mssm From The Muon Anomalous Magnetic Moment Measurement,” *Phys. Rev. D* **64** (2001) 075015 [arXiv:hep-ph/0104317].
- [96] T. Blazek and S. F. King, “Muon anomalous magnetic moment and $\tau \rightarrow \mu \gamma$ in a realistic string-inspired model of neutrino masses,” *Phys. Lett. B* **518**, 109 (2001) [arXiv:hep-ph/0105005].
- [97] M. Byrne, C. Kolda and J. E. Lennon, “Updated implications of the muon anomalous magnetic moment for supersymmetry,” *Phys. Rev. D* **67** (2003) 075004 [arXiv:hep-ph/0208067].
- [98] S. P. Martin and J. D. Wells, “Super-conservative interpretation of muon g-2 results applied to supersymmetry,” *Phys. Rev. D* **67** (2003) 015002 [arXiv:hep-ph/0209309].
- [99] S. Baek, P. Ko and J. h. Park, “Muon anomalous magnetic moment from effective supersymmetry,” *Eur. Phys. J. C* **24**, 613 (2002) [arXiv:hep-ph/0203251].
- [100] Heavy Flavour Averaging Group (HFAG), <http://www.slac.stanford.edu/xorg/hfag/>.
- [101] <http://www-cdf.fnal.gov/physics/new/bottom/bottom.html>.
- [102] T. Hurth, “Present status of inclusive rare B decays,” *Rev. Mod. Phys.* **75** (2003) 1159 [arXiv:hep-ph/0212304].
- [103] A. Dedes, “The Higgs penguin and its applications: An overview,” *Mod. Phys. Lett. A* **18**, 2627 (2003) [arXiv:hep-ph/0309233].
- [104] M. Carena, A. Menon, R. Noriega-Papaqui, A. Szynekman and C. E. M. Wagner, “Constraints on B and Higgs physics in minimal low energy supersymmetric models,” arXiv:hep-ph/0603106.
- [105] G. Jungman, M. Kamionkowski and K. Griest, “Supersymmetric dark matter,” *Phys. Rept.* **267** (1996) 195 [arXiv:hep-ph/9506380].
- [106] G. Bertone, D. Hooper and J. Silk, “Particle dark matter: Evidence, candidates and constraints,” *Phys. Rept.* **405** (2005) 279 [arXiv:hep-ph/0404175].
- [107] M. Drees, Y. G. Kim, T. Kobayashi and M. M. Nojiri, “Direct Detection Of Neutralino Dark Matter And The Anomalous Dipole Moment Of The Muon,” *Phys. Rev. D* **63** (2001) 115009 [arXiv:hep-ph/0011359].
- [108] E. A. Baltz and P. Gondolo, “Improved Constraints On Supersymmetric Dark Matter From Muon G-2,” *Phys. Rev. D* **67** (2003) 063503 [arXiv:astro-ph/0207673].
- [109] Y. G. Kim, T. Nihei, L. Roszkowski and R. Ruiz de Austri, “Upper and lower limits on neutralino

- WIMP mass and spin-independent scattering cross section, and impact of new $(g-2)_{\mu}$ measurement,” JHEP **0212** (2002) 034 [arXiv:hep-ph/0208069].
- [110] J. R. Ellis, K. A. Olive, Y. Santoso and V. C. Spanos, “Update On The Direct Detection Of Supersymmetric Dark Matter,” Phys. Rev. D **71** (2005) 095007 [arXiv:hep-ph/0502001].
- [111] D. N. Spergel *et al.*, “Wilkinson Microwave Anisotropy Probe (WMAP) three year results: Implications for cosmology,” arXiv:astro-ph/0603449.
- [112] R. Barate *et al.* [LEP Working Group for Higgs boson searches], “Search For The Standard Model Higgs Boson At LEP,” Phys. Lett. B **565** (2003) 61 [arXiv:hep-ex/0306033].
- [113] [Tevatron Electroweak Working Group], “Combination Of Cdf And D0 Results On The Mass Of The Top Quark,” arXiv:hep-ex/0603039.
- [114] LEP Electroweak Working Group (LEP EWWG),
<http://lepewwg.web.cern.ch/LEPEWWG/plots/summer2006/>.
- [115] M. Endo and T. Moroi, “Muon magnetic dipole moment and Higgs mass in supersymmetric SU(5) models,” Phys. Lett. B **525**, 121 (2002) [arXiv:hep-ph/0110383].
- [116] [ALEPH, DELPHI, L3, OPAL, SLD Collaborations], “Precision electroweak measurements on the Z resonance,” Phys. Rept. **427** (2006) 257 [arXiv:hep-ex/0509008];
<http://lepewwg.web.cern.ch/LEPEWWG/Welcome.html>.
- [117] S. Heinemeyer, W. Hollik, D. Stöckinger, A. M. Weber and G. Weiglein, “Precise prediction for $M(W)$ in the MSSM,” arXiv:hep-ph/0604147.
- [118] G. C. Cho and K. Hagiwara, “Supersymmetric contributions to muon $g-2$ and the electroweak precision measurements,” Phys. Lett. B **514** (2001) 123 [arXiv:hep-ph/0105037].
- [119] J. R. Ellis, S. Heinemeyer, K. A. Olive and G. Weiglein, “Indirect sensitivities to the scale of supersymmetry,” JHEP **0502** (2005) 013 [arXiv:hep-ph/0411216].
- [120] J. R. Ellis, S. Heinemeyer, K. A. Olive and G. Weiglein, “Phenomenological indications of the scale of supersymmetry,” JHEP **0605** (2006) 005 [arXiv:hep-ph/0602220].
- [121] S. Abel *et al.* [SUGRA Working Group Collaboration], “Report of the SUGRA working group for run II of the Tevatron,” arXiv:hep-ph/0003154.
- [122] S. Komine and M. Yamaguchi, “Bottom-tau unification in SUSY SU(5) GUT and constraints from $b \rightarrow s$ gamma and muon $g-2$,” Phys. Rev. D **65** (2002) 075013 [arXiv:hep-ph/0110032].
- [123] U. Chattopadhyay and P. Nath, “ b - tau unification, $g(\mu)-2$, the $b \rightarrow s + \text{gamma}$ constraint and nonuniversalities,” Phys. Rev. D **65** (2002) 075009 [arXiv:hep-ph/0110341].
- [124] U. Chattopadhyay and P. Nath, “Interpreting the new Brookhaven $g(\mu)-2$ result,” Phys. Rev. D **66** (2002) 093001 [arXiv:hep-ph/0208012].
- [125] H. Baer and C. Balazs, “ χ^2 analysis of the minimal supergravity model including WMAP, $g(\mu)-2$ and $b \rightarrow s\gamma$ constraints,” JCAP **0305** (2003) 006 [arXiv:hep-ph/0303114].
- [126] U. Chattopadhyay, A. Corsetti and P. Nath, “WMAP constraints, SUSY dark matter and implications for the direct detection of SUSY,” Phys. Rev. D **68** (2003) 035005 [arXiv:hep-ph/0303201].
- [127] J. R. Ellis, K. A. Olive, Y. Santoso and V. C. Spanos, “Likelihood analysis of the CMSSM parameter space,” Phys. Rev. D **69** (2004) 095004 [arXiv:hep-ph/0310356].
- [128] H. Baer, A. Belyaev, T. Krupovnickas and A. Mustafayev, “SUSY normal scalar mass hierarchy reconciles $(g-2)_{\mu}$, $b \rightarrow s\gamma$ and relic density,” JHEP **0406** (2004) 044 [arXiv:hep-ph/0403214].
- [129] B. C. Allanach and C. G. Lester, “Multi-dimensional mSUGRA likelihood maps,” Phys. Rev. D **73** (2006) 015013 [arXiv:hep-ph/0507283].
- [130] B. C. Allanach, “Naturalness priors and fits to the constrained minimal supersymmetric standard model,” Phys. Lett. B **635** (2006) 123 [arXiv:hep-ph/0601089].
- [131] A. Djouadi, M. Drees and J. L. Kneur, “Updated Constraints On The Minimal Supergravity Model,” JHEP **0603** (2006) 033 [arXiv:hep-ph/0602001].
- [132] J. Ellis, K. A. Olive and P. Sandick, “What if supersymmetry breaking appears below the GUT scale?,” arXiv:hep-ph/0607002.
- [133] S. Baek, P. Ko and W. Y. Song, “SUSY breaking mediation mechanisms and $(g-2)_{\mu}$,

- $B \rightarrow X_s l^+ l^-$ and $B_s \rightarrow \mu^+ \mu^-$,” JHEP **0303** (2003) 054 [arXiv:hep-ph/0208112].
- [134] G. F. Giudice and R. Rattazzi, “Theories with gauge-mediated supersymmetry breaking,” Phys. Rept. **322** (1999) 419 [arXiv:hep-ph/9801271].
- [135] E. Gabrielli and U. Sarid, “Low-energy signals for a minimal gauge-mediated model,” Phys. Rev. Lett. **79** (1997) 4752 [arXiv:hep-ph/9707546].
- [136] E. Gabrielli and U. Sarid, “Imminent phenomenology of a minimal gauge-mediated model,” Phys. Rev. D **58** (1998) 115003 [arXiv:hep-ph/9803451].
- [137] K. T. Mahanthappa and S. Oh, “Combined study of $b \rightarrow s\gamma$ and the muon anomalous magnetic moment in gauge-mediated supersymmetry breaking models,” Phys. Rev. D **62** (2000) 015012 [arXiv:hep-ph/9908531].
- [138] L. Randall and R. Sundrum, “Out Of This World Supersymmetry Breaking,” Nucl. Phys. B **557** (1999) 79 [arXiv:hep-th/9810155].
- [139] G. F. Giudice, M. A. Luty, H. Murayama and R. Rattazzi, “Gaugino mass without singlets,” JHEP **9812** (1998) 027 [arXiv:hep-ph/9810442].
- [140] J. L. Feng and T. Moroi, “Supernatural supersymmetry: Phenomenological implications of anomaly-mediated supersymmetry breaking,” Phys. Rev. D **61** (2000) 095004 [arXiv:hep-ph/9907319].
- [141] U. Chattopadhyay, D. K. Ghosh and S. Roy, “Constraining anomaly mediated supersymmetry breaking framework via ongoing muon $g-2$ experiment at Brookhaven,” Phys. Rev. D **62** (2000) 115001 [arXiv:hep-ph/0006049].
- [142] B. Lee Roberts [E821 Collaboration], “Muon ($g-2$): Past, present and future,” Nucl. Phys. Proc. Suppl. **155** (2006) 372 [arXiv:hep-ex/0510056].